Circumbinary Planets via Microlensing

Undergraduate Research Thesis

Presented in Partial Fulfillment of the Requirements for graduation "with Honors Research Distinction in Astronomy & Astrophysics" in the undergraduate colleges of The Ohio State University

by

Jacob Luhn

The Ohio State University

May 2015

Project Advisor: Professor B. Scott Gaudi, Department of Astronomy

Abstract

Circumbinary planets (planets that orbit around both members of a binary star system) have been the subject of many recent discoveries from Kepler data. Since their discovery, some focus has shifted to learning more about how these planets form. Many of the detected circumbinary planets have close orbits of 1 AU or less, since these are the planets that Kepler data are most likely to find. Circumbinaries with larger separations could provide insight into how these planets formed. Microlensing is a good technique to detect such planets due to its ability to detect small planets at large separations from their host. Here, we examine the parameter-space of wider circumbinary planets to see what circumbinary planet systems may look like as micrcolensing events, and we examine their caustic structures. These systems produce interesting caustic geometries in many cases. We also compare the movement of the caustics induced by the orbital motion of the binary star with the movement induced by the planet. Finally, we estimate a lower limit to the detectability of these circumbinaries in microlensing when the planet is very close to the Einstein radius.

Dedication

This thesis is dedicated to my parents, Perry and Kathleen,

whose love and support have been infinite;

and to my brother, Andrew,

whose scientific curiosity drives me to always learn more.

Acknowledgments

I am very grateful to the members of my committee, Dr. Scott Gaudi, Dr. Donald Terndrup, and Dr. Robert Perry for their time and expertise throughout this project and throughout my undergraduate career. They are the epitome of great advisors, always offering help and advice when asked.

I am especially thankful to Dr. Matthew Penny, who has spent countless hours guiding me through this project. His advice and mentoring has been invaluable to my growth as an astronomer. I also greatly appreciate his patience and willingness to answer the many questions I had. I am also grateful to Calen B. Henderson, who has always been available for comments and suggestions.

I wish to also thank the entire Department of Astronomy at The Ohio State University for providing a wonderful research environment. I would like to specifically thank Dr. Andy Gould who, although he is unaware, is responsible for sparking my interest in microlensing many years ago.

I am forever indebted to the Summer Undergraduate Research Program and its head Dr. Paul Martini for selecting me and providing the opportunity to conduct

this research. I am extremely grateful for everything they have done for my future career as an astronomer, which, without them, could not have gotten far.

Finally, I am thankful to all of the friends and family members who have supported and encouraged me throughout this process.

Table of Contents

List of Figures

Chapter 1: Introduction

1.1. Exoplanets

An extrasolar planet, or *exoplanet* is any planet that orbits a star other than the Sun. For a long time, the only known planets were those in our Solar System, and the existence of exoplanets was merely hypothesized. Over the centuries, we have learned that there is nothing unique about our Sun. In fact, it is just one of billions of other stars in the galaxy. Why, then, should the Sun be the only star with planets? And as we learned more about star formation and stellar life cycles leading to the formation of heavier elements, all signs pointed toward the existence of planets around other stars. The idea of planets beyond our solar system is one that has fascinated scientists and the public for years. With it comes the inevitable question: Is there life outside Earth? The concept of extraterrestrial life has been fantasized by many, but in order to get an understanding of what life may look like elsewhere, we need to answer the question: Is Earth special? To answer this question, we must search for exoplanets, and get an understanding of how common Earth-like planets are around Sun-like stars.

It was not until 1992 that the first confirmed discovery of an exoplanet occurred (Wolszczan & Frail 1992). Over the next few years, several more planets were discovered. Most of these planets were "hot Jupiters", meaning they are Jupiter-mass planets that orbit very close to their host star. However, with time and improved techniques, more varied exoplanets were soon found. Since the first discovery of an exoplanet, roughly 1900 more planets have been detected, proving that exoplanets are indeed very common. These planets can be found in a variety of systems: multiple planet systems, binary systems, etc. The discovery of multi-planet systems around Sun-like stars shows that our solar system is not unique, and there are hints that neither is the Earth.

As a rapidly-growing field, exoplanet science has quickly evolved into a number of different subfields. For a long time, much of the focus was on the search for exoplanets. This involved optimizing the various detection methods. Once exoplanets began to be discovered, the field turned toward characterizing these planets. As more diverse systems were discovered, people began to study the dynamics of planets by looking at complex systems like multi-planet systems for areas of stability and resonance. Naturally, there was always interest in habitability and finding Earth-like planets that may support life by looking at planets that would have temperatures similar to the Earth and examining exoplanet atmospheres. Another area of interest is in planet formation and how it compares with our ideas of star formation. Now that we have detected a large number of exoplanets, we can also look at the statistics of exoplanets and attempt to figure out how common planets are, typical sizes and separations of planets, and determine any biases. All of these subfields, however, rely on the initial step: being able to detect and characterize exoplanets to help provide confirmation to the theories they produce. Of course, detecting exoplanets is no easy task; there is no simple way to do so, and each method of detection has its advantages and disadvantages. There are four main methods of detecting exoplanets, which will briefly be explained here.

The *radial velocity*, or *Doppler*, method involves observing the absorption lines in the spectra of stars. If an observed star is host to a planet, the star and planet orbit around the center of mass of the system. As a result, the star will periodically move either toward or away from the Earth's line of sight (hence *radial* velocity). Therefore the emission lines of the star will be periodically blue- and red-shifted (hence *Doppler*). The period of this shift is the orbital period of the exoplanet. Thus, if we can measure or estimate the luminosity and distance of the star, we can infer the mass of the star, and by using the amplitude of the doppler shift, infer the mass and separation of the planet. The measured "wobble" of the star depends on the separation and mass of the planets. As a result, exoplanets that are more massive will tug more heavily on their host star, as will exoplanets that are in close orbits. This means that the radial velocity method is unfortunately biased toward high-mass, close-orbit exoplanets. In addition, the radial velocity method is sensitive

to viewing angle. The amplitude depends on the inclination i; therefore we do not measure the mass M, but $M \sin i$.

The *transit* method requires precise observation of the brightness of a star over a period of time. If the star hosts an exoplanet, the planet may periodically pass between our line of sight and the star during the course of its orbit. When this occurs, the star will appear slightly dimmer as the planet crosses it. After several of these transits, the period of the planet's orbit can be confirmed. Furthermore, the amplitude of the slight dip in brightness is proportional to the relative areas of the star and planet. Thus, if we can determine the size of the star, we can determine the size of the planet. These can be followed up with other measurements (radial velocity or transit timing) to determine the mass and separation of the planet. Like the radial velocity method, the transit method is more sensitive to large, close-orbit exoplanets, and requires an edge-on orbit.

The *microlensing* method is very different from the other two in the fact that we do not observe the light from the star or planet. Instead, it relies on a background star passing behind a foreground star relative to our line of sight. As it moves behind the foreground star, the gravitational field of the foreground star acts as a lens, perturbing the light from the distant star. The observed result is a magnification of the background star's brightness over the duration of the event, usually 10-30 days. When the lens star is host to a planet, the planet causes further perturbations and leads to sharp peaks in the magnification. By fitting the lightcurves (plots of brightness over time) with models, the exoplanet parameters can be obtained. Microlensing is unique in its ability to detect a wide range of planet masses at large separations. This makes it a powerful tool for exoplanet detection. Unfortunately, microlensing events are rare, as they rely on the chance alignment of a background and foreground star. In addition, the reliance on precise alignment means that the events are nonrepeating. Once a microlens event is complete, it will not be viewed again.

The final method is the *direct imaging* method. As its name suggests, this method requires directly imaging the exoplanet. At visible wavelengths, planets are very faint compared to their host stars. However, planets that are very hot will be

self-luminous, making them much brighter at infrared wavelengths, thus increasing their ability to be detected. However, this means that the planets must also be large enough to be seen, and also must be sufficiently separated from their host star so that the planet can be resolved.

The transit technique is responsible for the largest number of detected planets, closely followed by the radial velocity method. Microlensing is third with direct imaging not far behind, both an order of magnitude less than transit or radial velocity. Although detecting planets through microlensing is rarer than some of the other methods, its lack of bias toward close-orbiting, massive planets is what makes it the focus of this research. For this reason, the next section gives a more complete overview of the microlensing method, in order to better understand the concepts presented in this work.

1.2. Microlensing

What follows is a brief introduction to the basics of microlensing. It follows from the microlensing review found in Gaudi (2012). As described above, a microlensing event occurs when a background, or *source*, star passes behind a foreground, or *lens*, star. As the light of the source star passes the lens star, it gets bent by the gravity of the lens. The light from the source is then seen as multiple images. The mapping between the position of a source point and the resulting images is described by the *lens equation* in complex form

$$\zeta = z - \sum_{i}^{N_l} \frac{\epsilon_i}{\overline{z} - \overline{z}_{m,i}}, \tag{1.1}$$

where N_l is the number of masses in the lensing system, ζ is the position in complex coordinates of the source ($\zeta = x_s + iy_s$), z is the position of the image (the final position of the lightray after being bent) in complex coordinates, $\epsilon_i \equiv m_i/M_{tot}$, and $z_{m,i}$ is the complex position of mass i. The solution to the lens equation can be found analytically for $N_l = 1$, a single point mass. For a binary lens, the lens equation can be written as a fifth-order polynomial in z, which cannot be solved analytically and must instead be solved numerically. The magnification of a given image position is given by the inverse of the Jacobian determinant at that position. The determinant

of the Jacobian is

$$\det J = \det \begin{pmatrix} \frac{\partial \zeta}{\partial z} & \frac{\partial \zeta}{\partial \overline{z}} \\ \frac{\partial \overline{\zeta}}{\partial z} & \frac{\partial \overline{\zeta}}{\partial \overline{z}} \end{pmatrix} = 1 - \frac{\partial \zeta}{\partial \overline{z}} \frac{\overline{\partial \zeta}}{\partial \overline{z}}, \text{ where } \frac{\partial \zeta}{\partial \overline{z}} = \sum_i^{N_l} \frac{\epsilon_i}{(\overline{z} - \overline{z}_{m,i})^2}. \tag{1.2}$$

The *critical curves* define the set of image positions where $\det J = 0$, or where the magnification is formally infinite. From equation 1.2, this gives the condition

$$\left| \sum_i^{N_l} \frac{\epsilon_i}{(\overline{z} - \overline{z}_{m,i})^2} \right|^2 = 1, \tag{1.3}$$

which can be solved parametrically by

$$\sum_i^{N_l} \frac{\epsilon_i}{(\overline{z} - \overline{z}_{m,i})^2} = e^{i\psi} \tag{1.4}$$

for each value of $\psi = [0, 2\pi)$ (Witt 1990). This set of image positions where the magnification is infinite can be inserted back into the lens equation to map back to the source plane. This defines a set of closed, cuspy curves called *caustics* in the source plane. When the source star crosses the boundary to a caustic curve, a new pair of images is created and the magnification spikes. A sample caustic is shown in Figure 1.1, with a sample source trajectory and the resulting lightcurve. For a single lens ($N_l = 1$) at the origin, the caustic curve is a single point at the origin.

1.2.1. Planetary Microlensing

Microlensing is capable of detecting planets by detecting perturbations to the single-lens lightcurves. A planet perturbs the light rays that pass close to its position, given in units of the angular Einstein ring radius of the host lens,

$$\theta_{\rm E} \equiv \left(\frac{4GM}{D_{\rm rel} c^2} \right)^{1/2}, \tag{1.5}$$

where M is the mass of the host lens, $D_{\rm rel}^{-1} \equiv D_l^{-1} - D_s^{-1}$, and D_l and D_s are the distances to the lens and source. Typical source and lens distances when viewing toward the bulge of the Milky Way (e.g. 6 and 8 kpc, respectively) give the Einstein radius to be $[2-4] AU (M/M_\odot)^{1/2}$ (Gaudi 2012).

Planetary microlensing consists of a lens that has two components, where one is much less massive than the other. In these cases, the caustics appear in three different topologies, depending on the separation of the planet. When the planet's separation is less than the Einstein radius, the caustics take on the *close* topology. For planet separations that are very close to the Einstein radius, the caustics take on the *intermediate* or *resonant* topology. Finally, when the planet separation is much greater than the Einstein radius, the caustics take on the *wide* topology. These three topologies are explored in Figure 1.2, and shall be described in further detail in the following paragraphs.

In both the close and wide topologies, there is a four-cusped, arrowhead-shaped caustic located near the host star. This caustic is called the central caustic and its tip points toward the planet. Because of the similar size and shape of the central caustics in the close and wide topologies, it is often difficult to distinguish between these scenarios for planets detected through central caustic perturbations. However, because the caustic sizes are so small, only high magnification events (events where the source and lens reach a small angular separation) will result in these perturbations, and thus are relatively rare.

In the close topology, there are a total of three caustic curves. In addition to the central caustic, there are also two triangular caustics that appear on the opposite side of the host star from the planet. These two caustics are called planetary caustics, as they are associated with the planet. They also appear symmetrically across the planet-star axis. Their separation from the central caustic increases as the planet separation decreases. These caustics are generally small, and are comparable to the size of the central caustic. However, they increase in size as they move closer to the central caustic (i.e., as the planet separation grows close to the Einstein radius).

In the wide topology, there are only two caustic curves. Along with the central caustic, there is another planetary caustic. Although it is also called a planetary caustic, it is very different from the planetary caustics formed in the close topology. First, the wide topology planetary caustic is a single caustic that lies on the planet-star axis. Further, it lies on the same side of the host star as the

planet, and is between the two lenses. Finally, they contain four cusps in an astroid shape, instead of the three cusps seen in the planetary caustics of the close topology. Additionally, these caustics are generally significantly larger than the close topology planetary caustics.

In the intermediate topology, there is a single caustic curve. This single curve comes from the merging of the central caustic with the planetary caustic(s) in the close and wide topologies, and thus is called a resonant caustic. The resonant caustics are relatively large in size and contain six cusps. The large size gives it a large cross-section and is therefore more likely for a source to cross the resonant caustics.

Again, these three topologies are most easily understood by studying Figure 1.2.

1.3. Circumbinary Planets

A circumbinary planet is a planet that orbits two stars instead of a single star. Until recently, their existence was unknown and it was not certain if such planets could exist. Now, using data from the Kepler spacecraft, eight circumbinary planet systems have been discovered through the transit method, demonstrating that there exists a viable channel of planet formation around moderately close binary stars. Indeed, Armstrong et al. (2014) have estimated the abundance of circumbinary planets to be 10%, which is comparable to the abundance of planets around single stars. However, because the transit technique used by Kepler is sensitive to close-orbiting planets around close-orbiting binary stars, the circumbinaries discovered by Kepler have separations of only 1 AU or less. Finding planets in wider orbits or circumbinary planets around wider binaries requires a different technique. A search for circumbinary planets on wider orbits could shed light on whether they form in-situ (Meschiari 2014) or migrated inwards from a formation site further out (Kley & Haghighipour 2014).

Microlensing is sensitive to binary stars and both small and massive planets with separations on the order of 1 Einstein radius (1 $r_{\rm E}$), which is typically $\sim$2-4

AU. It also has the ability to find planets around lower-mass stars. However, it is not clear the extent to which a binary lens star might suppress or enhance the detectability of planets in the system. This is one goal of this project.

Figure 1.3 shows the eight circumbinary planetary systems found by Kepler. The shaded region shows the range of Einstein radii for varied distances to lens and source stars. Since the range of significant planetary microlensing sensitivity is $0.5 \rightarrow 2\ r_{\rm E}$ it is easy to see that microlensing would indeed be well-equipped to detect circumbinary planets with large separations (i.e. $1 \rightarrow 8$ AU).

The lightcurve of a microlensing event largely depends on the structure of the caustics. The appearance of caustics is a telltale sign of a system with more than one lens. The simplest cases are double-lens caustics (e.g., a star plus planet or binary star), which, with only two parameters (separation s, and mass ratio q), have been well studied (e.g. Mao & Paczynski 1991; Gould & Loeb 1992). Circumbinary planet systems consist of a planet orbiting around a binary star and are therefore triple-lens systems with more complicated caustics.

Triple-lens systems have been studied to some degree. Many studies concentrate on specific types of triple lens systems. For instance, several have studied the effects of microlensing in systems with a star and two planets (Gaudi et al. 1998; Han et al. 2001; Ryu et al. 2011; Song et al. 2013; Zhu et al. 2014). Two papers have focused on systems containing a binary star and single planet: Lee et al. (2008) studied wide binary systems where the planet orbits only one of the binary stars, and Han (2008) studied circumbinary systems of close-orbit binaries. The work done by Han (2008) estimates a range of planet and binary separations for which the microlensing technique is efficient in detecting the planetary systems. An expanded history of triple-lens studies is given in Danek & Heyrovsky (2015b). In addition, Danek & Heyrovsky (2015b) and the companion paper Danek & Heyrovsky (2015a) provide a systematic exploration of critical curve topologies and caustic geometries in several symmetric triple-lens models.

1.4. Scope of the Thesis

The work in this paper acts as a follow-up to the previous work on circumbinary planets in microlensing done by Han (2008). Specifically, it is the intent of this work to gain a deeper understanding of the caustic structures that might occur in circumbinary microlensing events. The structure of the caustics is crucial to the detectability of planets with the microlensing method. The detection probability for a planet is largely dependent on the shape, size, and location of the caustics. It is therefore important to understand how the caustics in circumbinary systems compare to the caustics in typical planetary systems. In Chapter 2 we highlight interesting features of the triple-lens circumbinary caustics. These features can be explored in further detail by looking through the collection of animations at `http://www.astronomy.ohio-state.edu/~luhn.5/animations/`, which allow for a more intuitive understanding of how varying individual parameters changes the caustic structure in circumbinary systems.

The position of the binary star plays are large role in the shape of the caustics. Given that the binary star is in a smaller orbit, and therefore has a smaller period, the orbit of the binary star may cause changes in the caustic structure during the course of a circumbinary microlensing event. Chapter 3 focuses on comparing the caustic movement induced by the orbital motion of the stellar binary and the caustic movement induced by the orbital motion of the circumbinary planet to see which would play a more pivotal role.

Chapter 4 examines the detectability of circumbinary systems over a limited range of parameters. This is done by defining a detection criterion for a single source trajectory, which can be averaged over all possible caustic crossing trajectories. This places a lower limit on the fraction of detectable trajectories for a number of circumbinary systems.

Chapter 5 summarizes the results of this work and contains a discussion of their implications for using the microlensing technique to detect circumbinary planets. Furthermore, it addresses areas for future work.

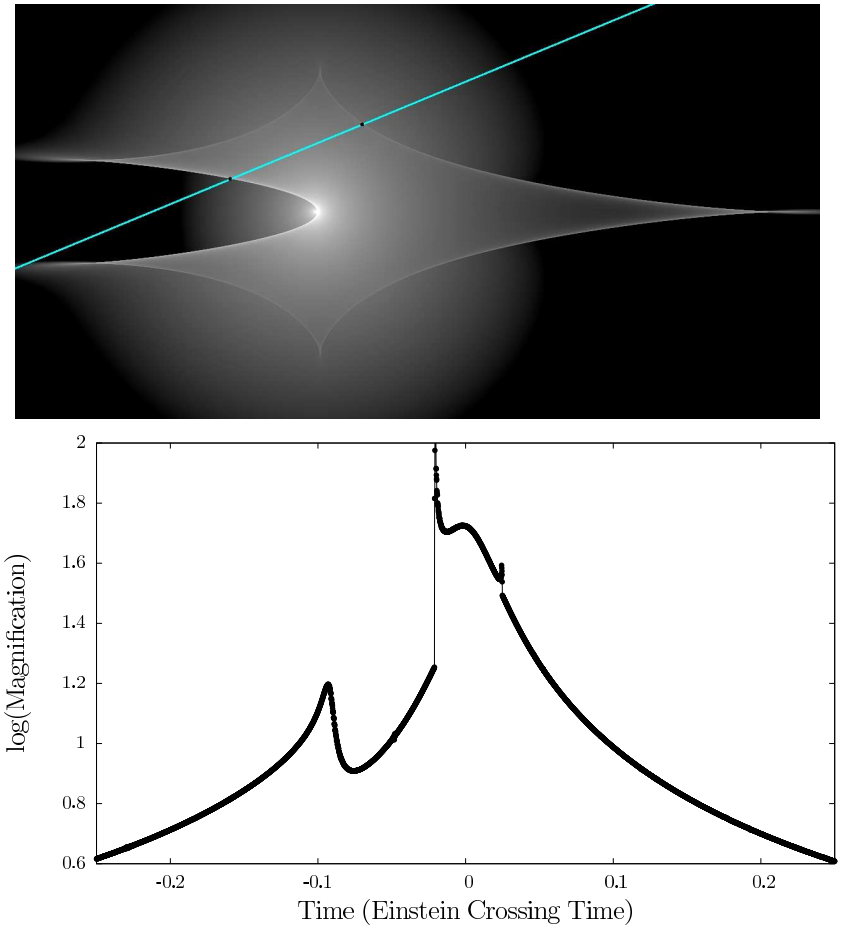

Fig. 1.1.— A sample caustic with a source trajectory and lightcurve. The top panel shows a magnification map, highlighting the outline of the caustic. Whiter areas are areas of higher magnification and darker areas are areas of lower magnification. The cyan line shows the trajectory of the source star (from bottom left to upper right). The two black points along the trajectory mark where it crosses the boundary to the caustic. The bottom panel shows the lightcurve that results from this trajectory. Note the relation between the caustic crossings of the trajectory and the peaks in the corresponding lightcurve. The first smooth peak in the lightcurve is not a caustic crossing, but is a caustic approach. The two sharp peaks in the middle are the two caustic crossings. The caustic plotted here is for a star-planet system with mass ratio 10^{-3} and separation 1 $r_{\rm E}$. The trajectory is defined by its closest approach, u_0 (0.02 $r_{\rm E}$), and its angle, α (22.5°).

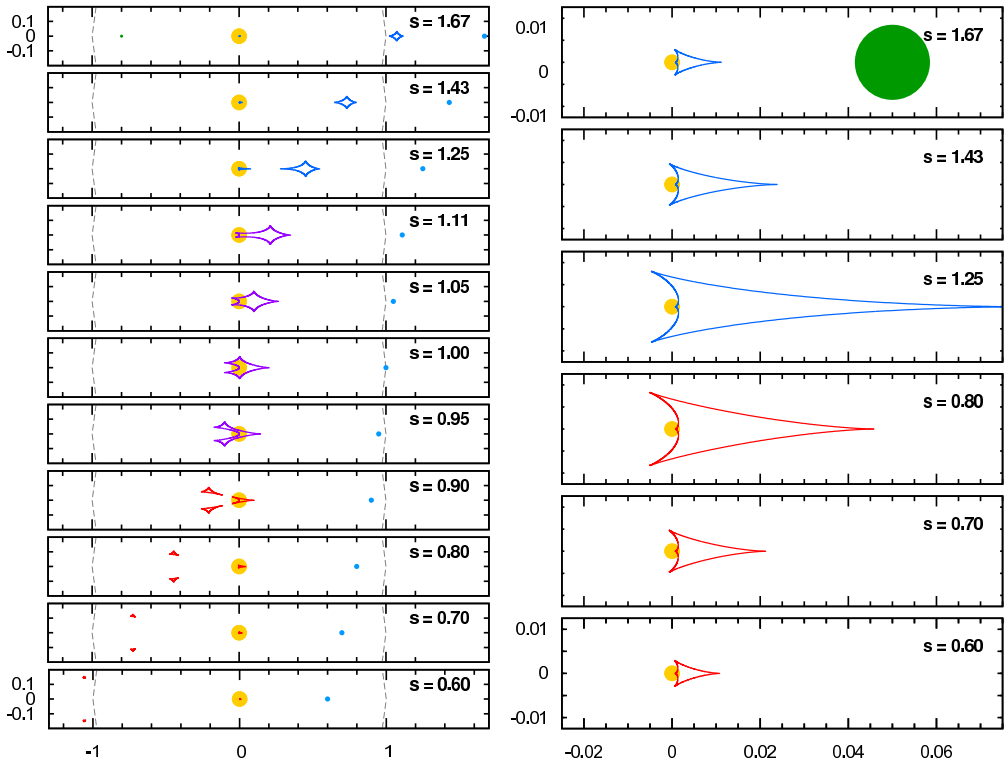

Fig. 1.2.— Caustic topologies in planetary microlensing. The red, purple, and blue curves show the caustic for a planetary lens with a mass ratio $q = 0.003$ for varying values of the planet separation, s in units of $r_{\rm E}$. The red curves are close topologies, the purple curves are intermediate topologies, and the blue curves are the wide topologies. The dotted grey curves show part of the Einstein ring. The yellow dots show the location of the host star, which is at the origin. The blue points show the location of the planet. The green dots in the topmost panels in both columns show a representative angular source size, which corresponds to a star with radius $\sim 13 R_\odot$ The right panels zoom in on the central caustics for the close and wide topologies. Adapted from *Exoplanets* by Sara Seager.

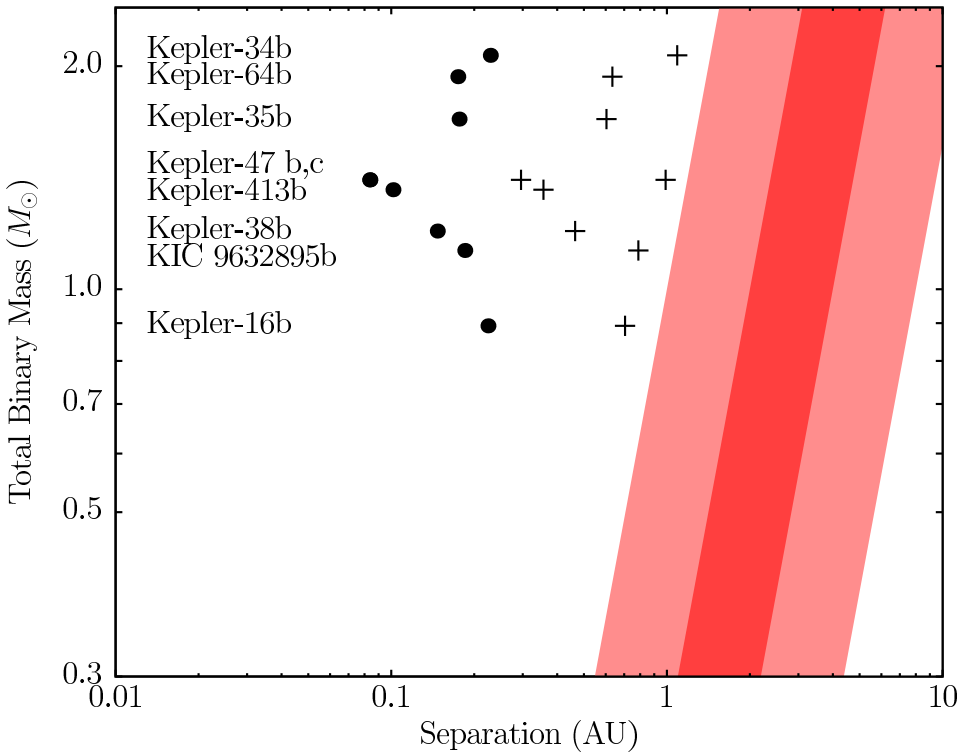

Fig. 1.3.— Stellar binary and circumbinary planet separations of the circumbinary systems from Kepler data. The large dots plot the separation between the two stars in the stellar binary. The crosses show the separation of the circumbinary planet(s) for each binary system. The dark red region shows the range of Einstein radii for typical lens and source distances when viewing toward the Bulge of the Milky Way. The light red region shows the range of microlensing's sensitivity (i.e. $0.5\ r_{\rm E} \rightarrow 2\ r_{\rm E}$).

Chapter 2: Gaining a Qualitative Understanding of Circumbinary Caustics

This chapter is devoted to highlighting unique features of circumbinary caustics. Understanding the structure of circumbinary caustics is an important first step to understanding potential circumbinary microlensing events. Of additional importance is understanding how the caustics change as various system parameters change. We find that the easiest way to gain an intuitive understanding of both of these is by creating a series of animations, showing the caustic structures across the large parameter space. The convenience of the animations is in the ability of a viewer to easily pick out unique features. The collection of animations can be viewed at `http://www.astronomy.ohio-state.edu/~luhn.5/animations/`. The details of the animations are discussed later in Section 2.2. However, it is first necessary to define the parameter space of circumbinary planets.

2.1. Circumbinary Parameter Space

A simple double-lens model (single star and planet system, or two star system) can be fully described by two parameters in microlensing: the mass ratio of the two bodies, q, and their separation, s. With triple-lens circumbinary planet systems, the additional lens increases the number of necessary parameters to five: the separation of the binary star, $s_{\rm b}$, the mass ratio of the binary star, $q_{\rm b}$, the separation of the planet, $s_{\rm p}$, the mass ratio of the planet to the total mass of the binary, $q_{\rm p}$, and the angle of the binary relative to the line connecting the planet to the center of mass of the binary, $\phi_{\rm b}$. We work in a coordinate system with the origin located at the *center of mass of the binary* and with the circumbinary planet located on the x-axis at a distance $s_{\rm p}$. This means that $\phi_{\rm b}$ is simply the angle of the binary from the x-axis. Figure 2.1 shows a diagram of the system and the parameters.

The large number of parameters makes it difficult to adequately explore the entire parameter space. For that reason, we made a collection of animations to quickly gain a more intuitive undersrtanding of how the caustics change as certain parameters change.

2.2. Animations

The range of parameters we explore is covered by 30 animations in the collection. Because double-lens systems consisting of a single star and single planet have been well studied, the animations are meant to highlight the features caused by the binarity of the two stars. As such, the animations show how the caustic structures change as the stellar binary parameters $\phi_{\rm b}$ and $s_{\rm b}$ change. The animations sample a range of five planet separations around the Einstein radius: $s_{\rm p} = 0.6, 0.95, 1.0, 1.05,$ and 1.5 $r_{\rm E}$. We additionally sample planet mass ratios of order Jupiter, to almost Earth-mass: $q_{\rm p} = 10^{-3}, 10^{-4}, 10^{-5}$. For each of these planet separations and mass ratios, there are two animations: one that shows how the caustics change as $\phi_{\rm b}$ goes from 0 to 2π, and another that shows how the caustics change as $s_{\rm b}$ goes from 0 to 0.4 $r_{\rm E}$. The upper limit for the binary separation is set by the stability limit for circumbinary planets given by Holman & Wiegert (1999). For our systems, face-on planets within 2.6 $s_{\rm b}$ will be unstable[1]. In each animation, the stellar binary mass ratio, $q_{\rm b}$ is unity.

2.2.1. Double-Lens Comparisons

The animations not only show how the circumbinary caustics change, but they also show a comparison between two double-lens systems, because the caustics from a general circumbinary planet triple-lens system can be well-approximated by two double-lens systems. The first double-lens system we compared them to is the system containing only the stellar binary, which we will call the *stellar double* system, or in shorthand: the AB system. (The shorthand notation is useful to avoid any confusion between the terms *stellar double* and *stellar binary*. Stellar binary refers to the binary star itself, whereas stellar double refers to the double-lens system used for

[1]However, since microlensing depends on projected separation, circumbinary planet separations within this limit are still allowed.

comparisons). The second double-lens system we compared them to is the system which includes the planet, but where the stellar binary has been replaced by a single star of the same total mass, located at the center of mass of the stellar binary, which we will call the *planetary double* system, or Ab system. These two double-lens systems are important to understanding the full triple-lens circumbinary system (called *circumbinary triple*, or ABb, system) because the caustics produced from the ABb system are often well-approximated by a superposition of the AB and Ab systems (Han 2008). The animations look heavily at the comparisons between the *circumbinary triple* system and the two double-lens approximations since much of microlensing is focused on detecting double-lens systems. These comparisons should be able to give a qualitative idea of whether the triple-lens circumbinary system would be detected as such or if it could be mistaken for one of these double-lens systems. Figure 2.1 can be used to show the three systems that are compared here: ABb, AB, and Ab. The three points represent the full ABb system. The AB system can be seen by taking away the planet (smaller point), leaving the two larger points. The Ab system can be seen by taking the two large points and replacing them with a point at the **X**.

2.2.2. Understanding the Animations

Figure 2.2 shows a sample screenshot of an animation. Each animation has four panels. The first panel in the top left, gives an overview of the all of the caustics except two: for each set of caustics, there are two caustics due to the stellar binary at $x \sim 0$ (when $\phi_{\rm b} \sim 0$) that are located symmetrically around the x-axis at several Einstein radii, which cannot be viewed in the first panel without making the other caustics impossible to see. The window of the first panel is constant, and does not change. The second panel (top right) shows the central caustic region, usually of the stellar binary. In the $\phi_{\rm b}$ animations, the window stays fixed. However, in the $s_{\rm b}$ animations, the window zooms in and out to keep the central caustic from the stellar binary a fixed size; occasionally it will shift positions. The third panel (bottom left) focuses on the planetary caustics. In the cases where there are two planetary caustics, this panel focuses on only one of them, since the other moves in a similar way. For the $\phi_{\rm b}$ animations, this window stays in a fixed position. For the

$s_{\rm b}$ animations, the window stays a fixed size but moves to keep the ABb planetary caustic in the center of the window. This is done to highlight changes in the size of the caustics. The final panel focuses on the lower of the two far triangular caustics from the stellar binary that are not shown in the first panel. In both $s_{\rm b}$ and $\phi_{\rm b}$ animations, the window stays a fixed size, but moves so that the caustic remains in the center of the window. In each panel, it is important to take note of the axes and how they are changing; this is the easiest way to understand what each window is doing.

The animations provide an efficient way to explore the circumbinary parameter-space. What follows is a description of the interesting features we observed from the animations.

2.3. Superposition

What is immediately noticeable from the animations is the fact that the ABb system is well-approximated by a superposition of the AB and Ab systems, as previously noted by Han (2008), and similarly noted for multiplanet systems by Gaudi et al. (1998) and Han et al. (2001). In fact, the ABb caustics appear to cloesly follow the three topologies of double-lens planetary microlensing, though see Danek & Heyrovsky (2015a) for a more precise definition of the multiple possible topologies of the triple lenses.

As described in 1.2.1, double-lens microlensing events with a single star and a single planet can be described as *close* (separation of the planet is less than 1 $r_{\rm E}$), *resonant* (separation of the planet is very close to 1 $r_{\rm E}$), and *wide* (separation of the planet is greater than 1 $r_{\rm E}$). For the most part, the ABb systems studied here have the same close, resonant, and wide characterizations that depend on the separation of the circumbinary planet, and so we will use this same terminology to describe the ABb topologies.

The superposition is not always an exact superposition. It is usually most helpful as a good first assumption. In the cases where the AB and Ab systems have caustics in the same location, the ABb caustic is dominated by the system with the

larger caustic (AB or Ab). However, in situations where the AB and Ab caustics are approximately the same size, the resulting ABb caustics begin to self-intersect and contain swallowtail catastrophes. The catastrophes are where the superposition begins to break down.

The caustics from double-lens systems are non-intersecting. The catastrophes in double-lens systems are simply the folds and cusps. Triple-lens caustics, however, are free to self-intersect. In addition, they can contain higher order catastrophes. There are two types of higher order catastrophes that can occur from triple-lens systems: butterfly, and swallowtail (Danek & Heyrovsky 2015b). The swallowtail catastrophe is seen more often in the circumbinary systems than the butterfly catastrophe, and so it will be examined more closely.

The swallowtail catastrophes occur in resonant circumbinary systems when the stellar double component is sufficiently large. For these topologies, the overall ABb resonant caustic is a superposition of the six-cusped Ab resonant caustic, and the central four-cusped AB astroid caustic. However, the swallowtail catastrophes do not always occur, and instead depend on the angle of the stellar binary, $\phi_{\rm b}$. For the $s_b = 0.2\ r_{\rm E}$ resonant caustic, at $\phi_{\rm b} = 0°$, there are two swallowtails. As $\phi_{\rm b}$ increases, the top swallowtail shrinks in size, and the bottom swallowtail increases in size, gaining one of the cusps of the stellar binary caustic. At $\phi_{\rm b} = 45°$, the top swallowtail is destroyed, leaving the three-cusped region from the former bottom swallowtail. At $\phi_{\rm b} = 135°$, the three-cusped caustic decreases in size as the bottom swallowtail is created again. As $\phi_{\rm b}$ increases, the three-cusped region loses a cusp and returns back to the original top swallowtail. Figure 2.3 shows the bottom swallowtail being reformed around $\phi_{\rm b} = 135°$.

Even for the range $45° < \phi_{\rm b} < 135°$ when there are no swallowtails, the caustic still contains self-intersections and an unusual three-cusped region. It is likely that a source trajectory that passes over these regions will contain strange features in the lightcurve. Additionally, the large size of the caustics increases the likelihood that a trajectory will encounter one of these regions. Therfore, the resonant caustics are perhaps the most likely systems to be recognized as circumbinary systems. In chapter 4 we examine resonant caustics in the context of detectability.

Now that we have briefly examined the resonant topology, we will look at the close and wide topologies, beginning with the central caustics.

2.4. Central Caustics

Central caustics appear in all three topologies: close, resonant, and wide. However, as discussed in the previous section, the central caustic of the resonant topology is much larger than the central caustic in the close and wide topologies. Because of this large difference in the size, the central caustics of the close and wide topologies behave differently, and shall be discussed here.

In addition to the size difference, the central caustics of the Ab system are also shaped differently. When in the close and wide topologies, the central caustics of the Ab system are four-cusped, arrowhead-shaped caustics, unlike the central resonant caustic, which has six cusps. Although the AB caustics are still astroid-shaped with four cusps, the superposition of the astroid with the arrowhead behaves differently than the superposition of the six-cusped resonant shape and the astroid.

For this reason, the swallowtail catastrophes occur with less frequency in the close and wide topologies. When a swallowtail appears, the resulting ABb caustics are significantly different from those of the two double-lens approximations. It would appear that, for the same reasons described at the end of 2.3, such caustics could be identifiable as triple-lens systems. However, because the caustics themselves are smaller, these swallowtails are significantly smaller and it is even less likely for a source trajectory to pass over them. In addition, these extra cusps from the swallowtail catastrophe are not present for angles of ϕ_b close to 0°. These smaller angles require a closer look and a different approach.

For angles of ϕ_b close to 0°, it is the shape of the ABb caustic that is interesting. For these small angles, the caustic has only four cusps and does not self-intersect, which make it very similar to the central caustics in the two double-lens approximations.

The overall shape of the ABb caustic is determined by which of the two double-lens central caustics is dominant: when the central caustic of AB is larger

than the central caustic of Ab, the shape of the central caustic looks more like the central caustic of AB, and vice versa. Figure 2.4 shows the progression of the ABb central caustics from AB dominated to Ab dominated. If a source passes over a caustic where the central caustic shape is dominated by one of the double-lens approximations, then it would be hard to recognize the system as a triple-lens system.

The sizes of the double-lens central caustics depend on $s_{\rm p}$ and $s_{\rm b}$. For a given value of one, there is a small range of values for the other where they produce central caustics that are roughly the same size. When this happens, the shape of the central caustic of the triple-lens system is intermediate to that of the two double-lens central caustic shapes and neither is dominant. For these cases, the intermediate shape contains the overall shape of the central caustic from AB, but one cusp has been elongated to more closely match the central caustic of the Ab. This shape is unusual for a central caustic and if a source passes over such a caustic, it is reasonable to predict that the elongation would be recognizable (provided that the trajectory crossed from the AB-like part to the Ab elongated part), and the system would therefore be recognizable as a circumbinary planet system. However, it is important to keep in mind that the central caustics in the close and wide topologies are very small and as such, it is less likely for a source to pass directly over one of these caustics. In addition, with small caustics, finite source effects may either aid recognition by probing more of the caustic, or hinder recognition by smoothing out the lightcurves.

2.5. Planetary Caustics

The location of the planetary caustics in the ABb system are largely set by their location in the Ab system. As their name suggests, the location of the planetary caustics mostly depend on the location of the planet (circumbinary planet in the ABb system). However, from viewing the animations, it is clear that the position of the caustics in the ABb system is also strongly affected by the stellar binary parameters $\phi_{\rm b}$ and $s_{\rm b}$. In this section, we will highlight how changing these stellar parameters affects the position of the planetary caustics.

2.5.1. Effects of Changing Stellar Binary Angle (ϕ_b)

As ϕ_b goes through a full rotation, the planetary caustics translate in a circle around a point. The point is the location of the planetary caustic in the Ab system. This motion is evident in the close topology in Figure 2.5 and in the wide topology in Figure 2.6. What is not as evident in the figures but is clearly seen in the animations is the correlation between the translation of the caustic and the revolution of the stellar binary: as the stellar binary roates counter-clockwise, the planetary caustic moves clockwise. This motion of the planetary caustics is consistent across the close, and wide topologies. Even in the resonant cases, the planetary caustics join together with the central caustics to form one caustic. For these caustics, the sections of the caustic that came from the planetary caustics continue to move in this fashion as ϕ_b changes. The radius of translation of the planetary caustics is greatest when the planet is in the close topology, and decreases as the planet moves further out. Again, this is seen in Figures 2.5 and 2.6. In the wide topology (Figure 2.6), the radius of translation is much smaller than in the close topology. In addition to the translation, there is a slight change in size, as shown in the bottom panels of each figure.

2.5.2. Effects of Changing Stellar Binary Separation (s_b)

By varying s_b, the planetary caustics undergo a different translation. In this case, however, they are not moved in a circle but instead are translated in a straight line. Once again, this movement is based around the planetary caustic position of the Ab system. As expected, when the separation of the stellar binary, s_b, is 0, the ABb system is indistinguishable from the Ab system (since this is how we defined the Ab system). As s_b increases from 0, the caustics of the circumbinary system are translated away from their position at 0 (and away from the star and planet). The translational movement is mostly observed in the close and wide topologies. In addition to the translational movement, there is a change in size that occurs in the close topologies. As the caustics move farther away from their position at $s_b = 0$, they also shrink in size. In the wide topology, the the caustic stays roughly the same size throughout the translation. These feautures are highlighted in Figures 2.7 and 2.8.

The previous sections have highlighted a number of features viewable in the animations of the ABb caustics. While the animations are mainly meant to give a more intuitive understanding of how the ABb caustis depend on the stellar binary parameters $\phi_{\rm b}$ and $s_{\rm b}$, they can also be used as crude simulations of the orbital motion of the stellar binary. With this in mind, it is clear that the orbital motion of the stellar binary can induce significant changes in the shape and/or position of the planetary caustic. The next chapter discusses this phenomenon and places it into context, comparing it to the changes induced by the orbit of the planet.

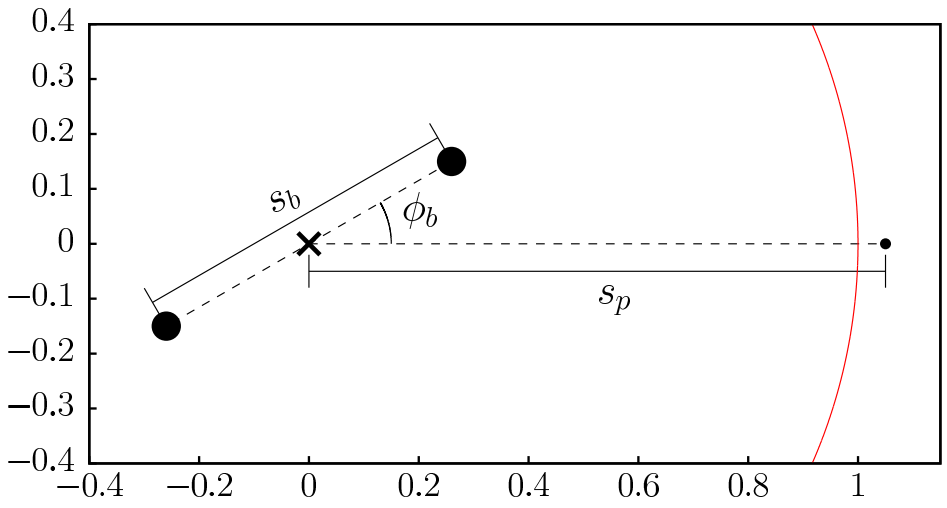

Fig. 2.1.— Diagram showing the coordinate system and parameters used for calculations. The thick X marks the center of mass of the stellar binary - note that this is not the center of mass of the whole 3-body system. The red circle indicates the Einstein ring. The sizes of the binaries and planet are not to scale. Units are units of the Einstein-radius, $r_{\rm E}$.

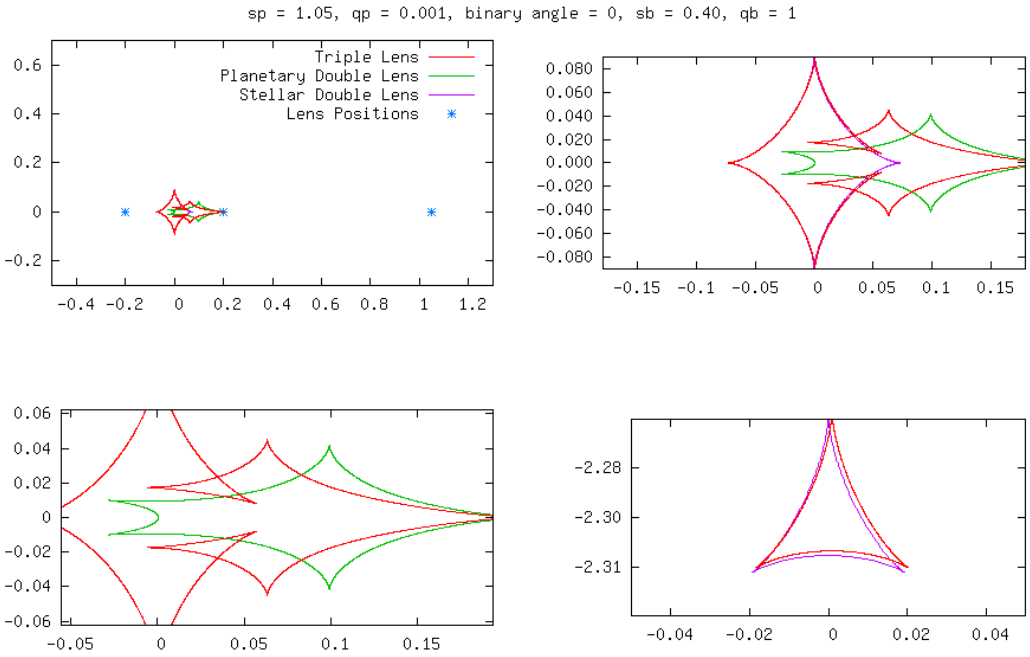

Fig. 2.2.— Screenshot of an animation used to show comparisons of the caustics between the circumbinary triple ABb (red); stellar double AB (magenta), and the planetary double Ab (green). The top left panel shows the whole system (except for two of the stellar binary caustics which are located above and below the window). The top right panel zooms in on the central caustic. The bottom left panel zooms in on one of the two planetary caustics. The bottom right panel zooms in on one of the two stellar binary caustics which were not shown in the top left panel.

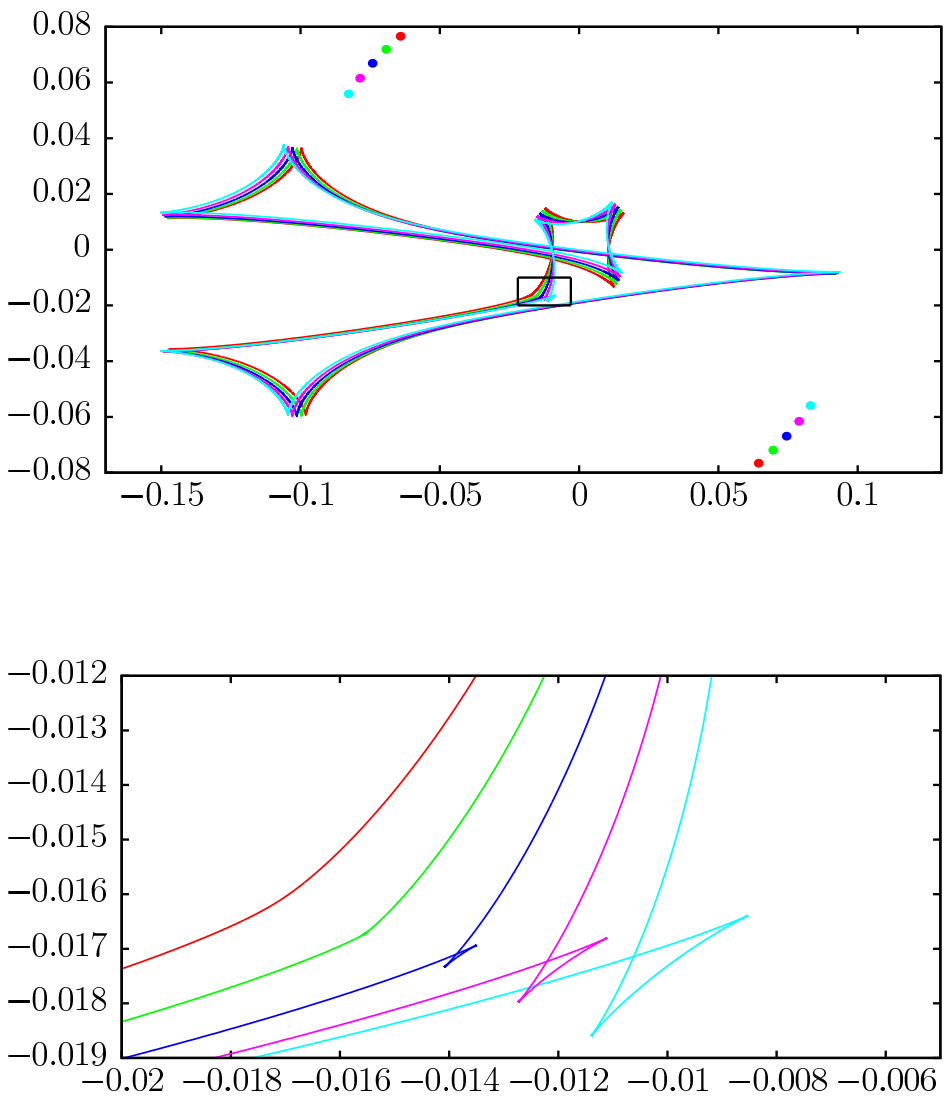

Fig. 2.3.— Creation of a swallowtail catastrophe in the resonant central caustic as $\phi_{\rm b}$ changes. The top panel shows the full central caustic while the bottom panel zooms in on the boxed region to show creation of a swallowtail. The colored points on the top panel show the position of the stellar binary lenses as $\phi_{\rm b}$ changes from 130° (red) to 146° (cyan). The colors of the points correspond to the stellar binary positions of the same-colored caustic. Here $s_{\rm b} = 0.2\ r_{\rm E}$, $s_{\rm p} = 0.95\ r_{\rm E}$, $q_{\rm b} = 1$, and $q_{\rm p} = 10^{-3}$

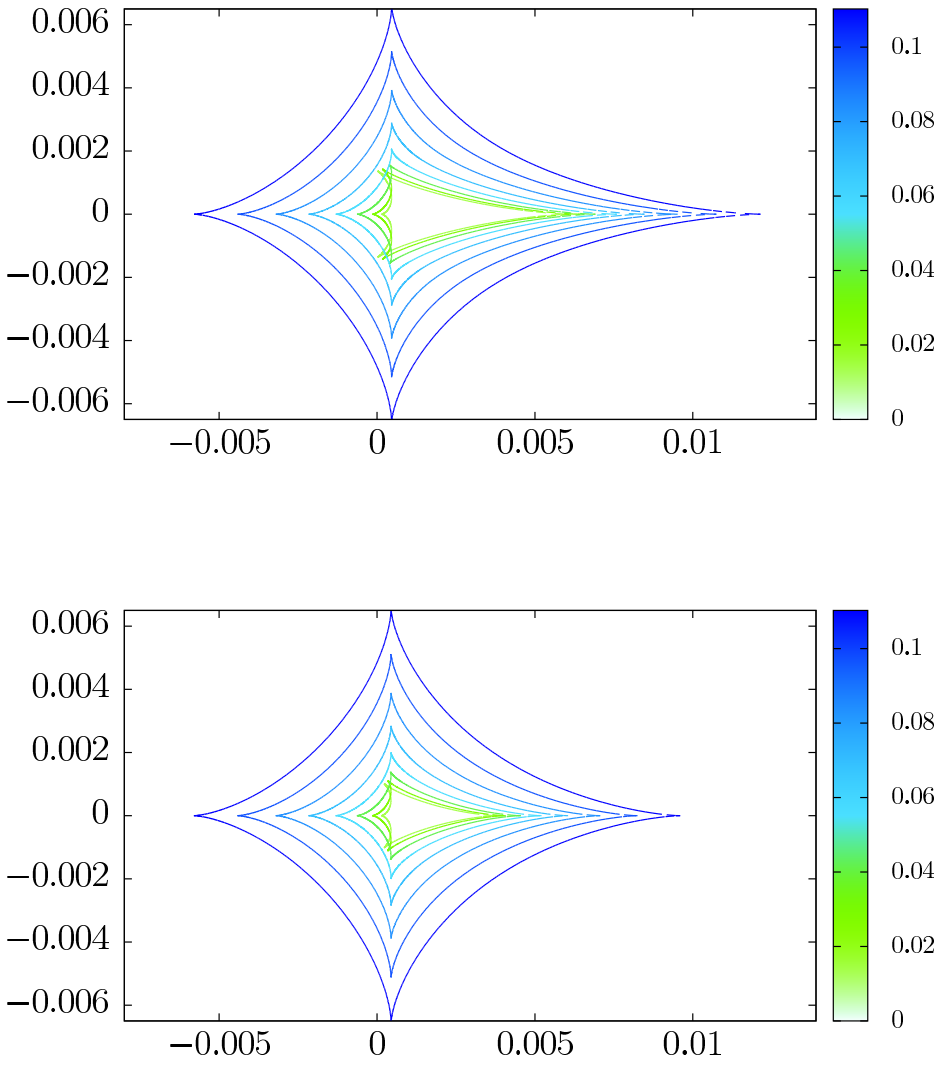

Fig. 2.4.— Central caustics of the close and wide topologies as $s_{\rm b}$ varies. The color palette shows the approximate value of $s_{\rm b}$. The caustics of importance are in the middle of the color region and show the caustic shape intermediate to those from the AB and the Ab systems. The top panel shows the central caustic of a close topology ($s_{\rm p} = 0.6$), and the bottom panel shows the central caustic of a wide topology ($s_{\rm p} = 1.5$).

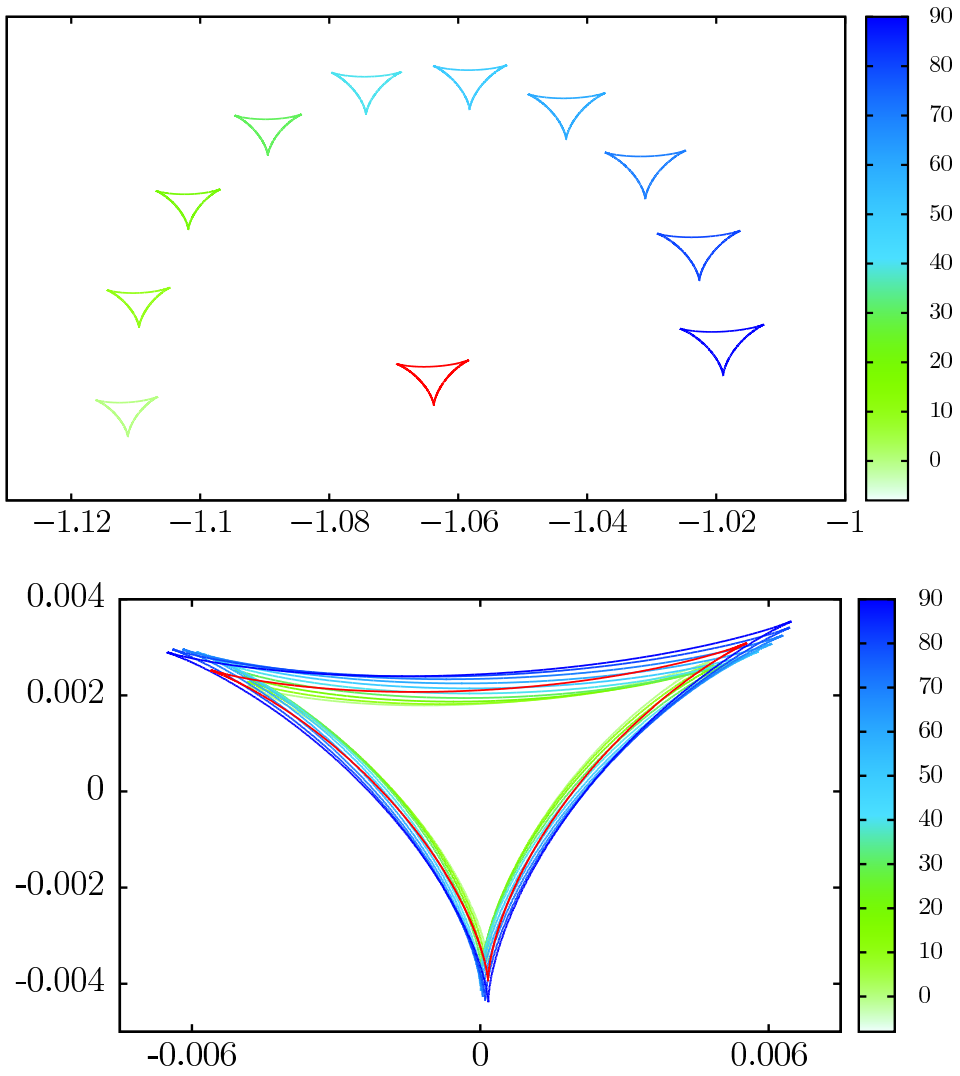

Fig. 2.5.— Effect of changing $\phi_{\rm b}$ on planetary caustics in close topology. The colored caustics are the triple-lens circumbinary caustics at various values of $\phi_{\rm b}$. As the color goes from green to blue, $\phi_{\rm b}$ increases. The red caustics show the Ab caustics. The two top panel shows the actual caustic positions in the source plane. The bottom panel shows the same caustics overlaid on one another to show the slight change in size and shape. Note that the caustics are displace by 180° for stellar binary displacement of 90°

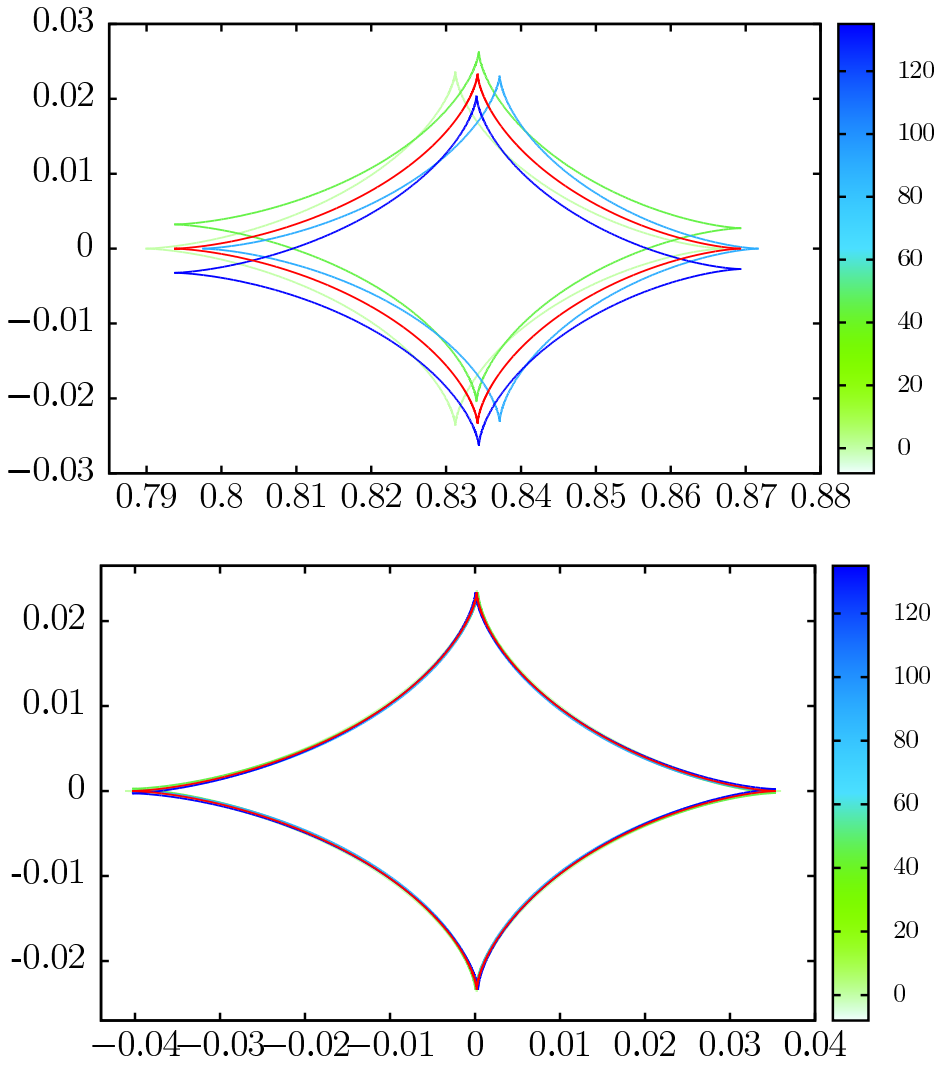

Fig. 2.6.— Effect of changing ϕ_b on planetary caustics in wide topology. The colored caustics are the triple-lens circumbinary caustics at various values of ϕ_b. As the color goes from green to blue, ϕ_b increases from 0° to 180°. The red caustics are the Ab caustics. The top panel shows the actual caustic positions in the source plane. The bottom panel shows the same caustics overlaid on one another to show the slight change in size and shape. In this case, the change is miniscule.

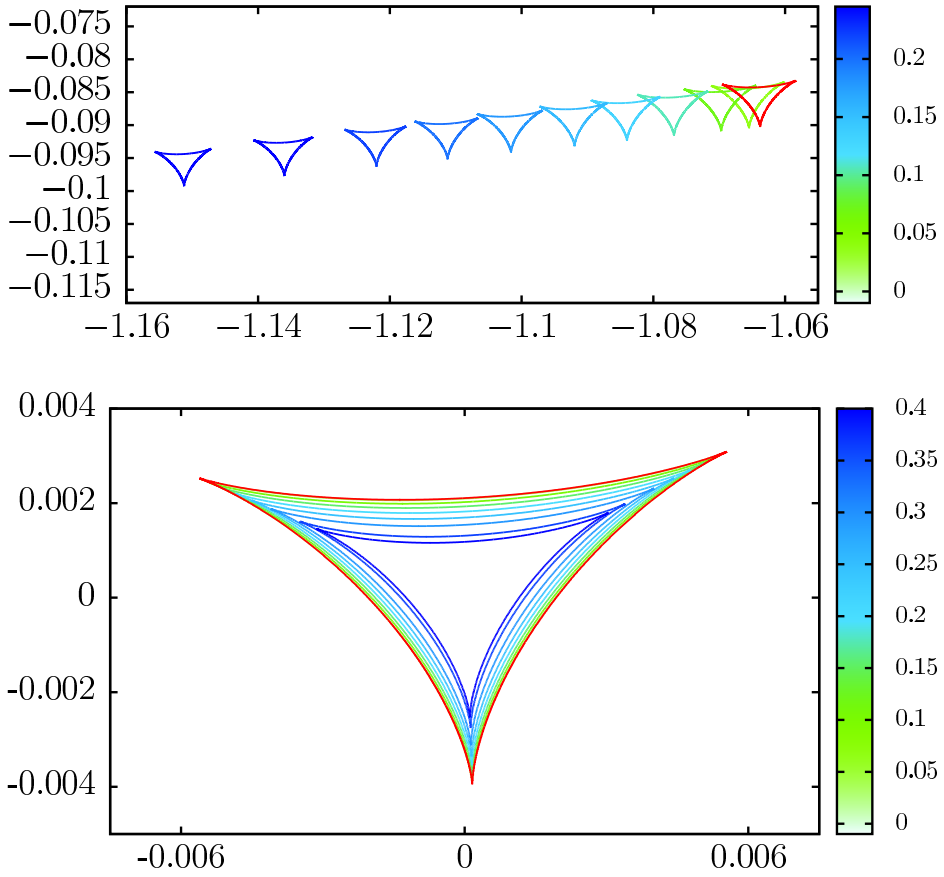

Fig. 2.7.— Effect of changing $s_{\rm b}$ on planetary caustics in close topology. The colored caustics are the triple-lens circumbinary caustics at various values of $s_{\rm b}$, indicated by the color palette. The red caustics are the Ab caustics. The top panel shows the actual caustic positions in the source plane. The bottom panel shows the same caustics overlaid on one another to show the slight change in size and shape. Note that in the top panel, $s_{\rm b}$ ranges from 0 to 0.2 $r_{\rm E}$ to show the displacement of the caustics. The bottom panel overlays the caustis for $s_{\rm b}$ values ranging from 0 to 0.4 $r_{\rm E}$. The difference in size is much grater for changes in $s_{\rm b}$ than for changes in $\phi_{\rm b}$ (Figure 2.5).

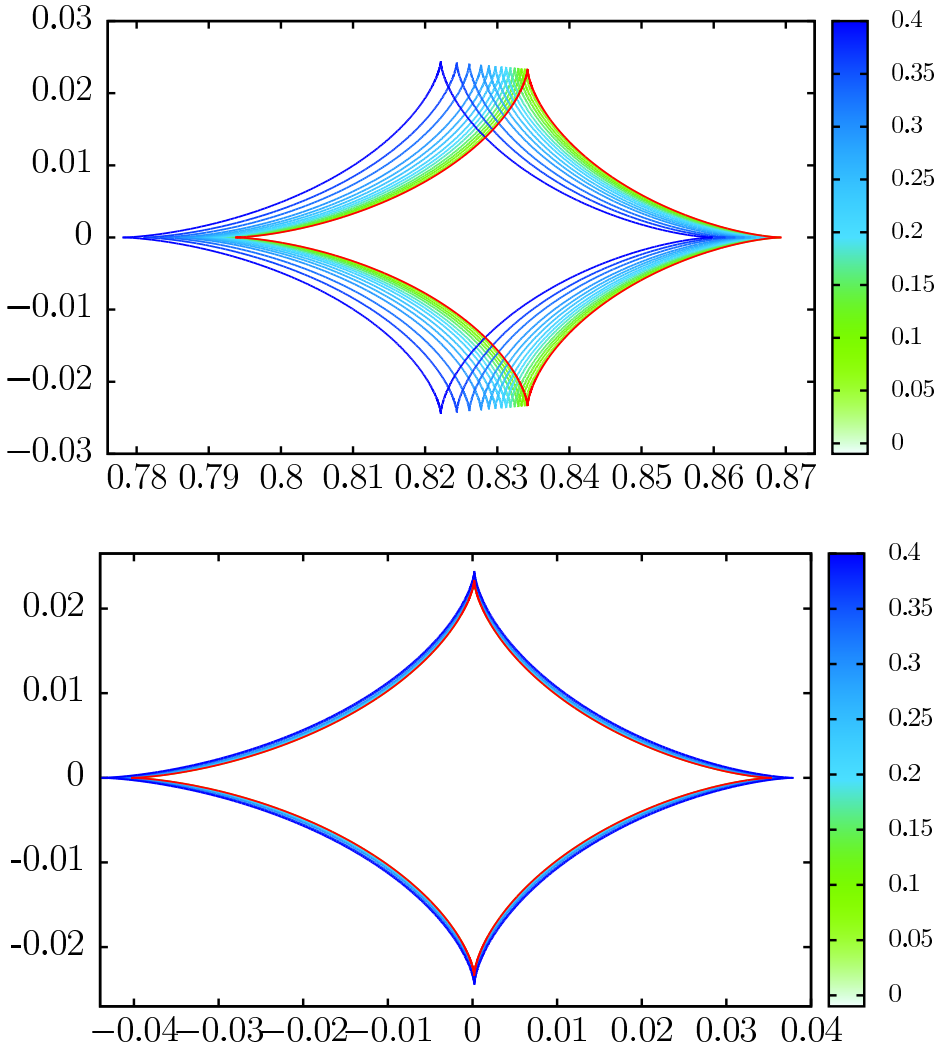

Fig. 2.8.— Effect of changing $s_{\rm b}$ on planetary caustics in wide topology. The solid caustics are the triple-lens circumbinary caustics at various values of $s_{\rm b}$, indicated by the color palette. The red caustics are the Ab caustics. The top panel shows the actual caustic positions in the source plane. The bottom panel shows the same caustics overlaid on one another to show the slight change in size and shape. Here, $s_{\rm b}$ ranges from 0 to 0.4 $r_{\rm E}$ in both panels. Note that the change in size of the caustics is again very small (as with changing $\phi_{\rm b}$, seen in Figure 2.6).

Chapter 3: Orbital Motion of Stellar Binary

In some planetary microlensing events, the time it takes the source to cross the Einstein radius can be long enough that the orbital motion of the planet can be detected due to the change it induces on the caustic features (e.g. Dominik 1998; Ioka et al. 1999; Albrow et al. 2000; Penny et al. 2011). With this fact in mind, after looking at how the stellar binary of our triple-lens system can affect the shape, size, and position of the caustics, it becomes reasonable to expect that the orbital motion of the stellar binary could be detected in a similar fashion. After all, the stellar binary is on a closer orbit than the planet, and would therefore have a faster angular velocity. An easy way to see if this could be detected is to compare the movement of the caustic due to changes in stellar-binary parameters $\phi_{\rm b}$ and $s_{\rm b}$ with the movement of the caustic due to changes in planetary parameters $s_{\rm p}$. This requires quantification of some of the qualitative features discussed in section 2.5. Orbits will in general be inclined and eccentric, but for simplicity, we examine only circular orbits either face- or edge-on.

3.1. Face-on

When face-on, the orbital motion of the stellar binary corresponds to $\phi_{\rm b}$ changing, and the orbital motion of the circumbinary planet corresponds to a rotation of the whole frame (x-axis in Figure 2.1).We define a quantity Ω to be the movement of the planetary caustic induced by the orbital motion of the stellar binary as a fraction of the movement induced by the orbital motion in the planetary double scenario. This is given by Equation 3.1:

$$\Omega \equiv \frac{\left(\frac{dr_{\rm pc}}{dt}\right)_{\rm b}}{\left(\frac{dr_{\rm pc}}{dt}\right)_{\rm p}} \tag{3.1}$$

where the subscript F indicates face-on observing and $r_{\rm pc}$ is the position of the planetary caustic.

We can estimate $\frac{dr_{\rm pc}}{d\phi_{\rm b}}$, the average distance traveled by the planetary caustic per degree change in $\phi_{\rm b}$, by computing the center position of the caustic at each angle $\phi_{\rm b}$ and averaging the change in this position between each angle [1]. Then we calculate a similar expression to describe the average distance traveled by the planetary caustic per degree that the planet rotates, $\frac{dr_{\rm pc}}{d\phi_{\rm p}}$. Because the caustic itself is not changing as $\phi_{\rm p}$ changes, $\frac{dr_{\rm pc}}{d\phi_{\rm p}}$ is a constant and equals $\frac{2\pi r_{\rm pc}}{360}$. However, because the stellar binary has a shorter orbital period than the planet, they will not move by the same angle in the same amount of time. To get a ratio of these two factors in terms of time, we calculate their angular velocities. Equation 3.1 shows how we can obtain $\Omega_{\rm F}$.

$$\Omega_{\rm F} = \frac{\frac{dr_{\rm pc}}{d\phi_{\rm b}}\frac{d\phi_{\rm b}}{dt}}{\frac{2\pi r_{\rm pc}}{360}\frac{d\phi_{\rm p}}{dt}} = \frac{\frac{dr_{\rm pc}}{d\phi_{\rm b}}}{\frac{2\pi r_{\rm pc}}{360}}\frac{\omega_{\rm b}}{\omega_{\rm p}} \tag{3.2}$$

Finally, we can use the fact that the ratio of the angular velocities will only depend on the ratio of separations,

$$\frac{\omega_{\rm b}}{\omega_{\rm p}} = \left(\frac{s_{\rm p}}{s_{\rm b}}\right)^{\frac{3}{2}}, \tag{3.3}$$

with the $\frac{3}{2}$ power coming from Kepler's third law, so that

$$\Omega_{\rm F} = \left(\frac{\frac{dr_{\rm pc}}{d\phi_{\rm b}}}{\frac{2\pi r_{\rm pc}}{360}}\right)\left(\frac{s_{\rm p}}{s_{\rm b}}\right)^{\frac{3}{2}}. \tag{3.4}$$

These ratios were calculated for various $s_{\rm b}$ and $s_{\rm p}$ values. Figure 3.1 shows the results for the face-on case. First, the motion of the caustic due to the orbit of the planet is larger for nearly all values of $s_{\rm b}$ and $s_{\rm p}$. The only case where the stellar binary induces more motion of the planetary caustic is in the resonant topologies. Another point to take away is that for a given $s_{\rm b}$ value, as $s_{\rm p}$ approaches 1 $\Omega_{\rm F}$ gets larger. This is because the orbit of the stellar binary merely causes the planetary caustic to translate in a circle around a fairly close point whereas the orbit of the planet causes the caustic to rotate around the center of mass of the system.

[1] The center position was taken to be the average position of caustic points equally spaced in ψ, from Equation 1.4.

3.2. Edge-on

A similar calculation was performed for the edge-on scenario. In this case, we calculated how much the planetary caustic moves as $s_{\rm b}$ varies. However, for this calculation, we needed to find $\frac{dr_{\rm pc}}{ds_{\rm b}}$. This was approximated by finding the distance moved by the caustic as $s_{\rm b}$ was changed by $\pm 1\%$. In order to campare how much the planetary caustic moves due to the stellar binary to how much it moves due to the planet it is necessary to know how they change in the same amount of time. Instead of multiplying by the angular velocity $\frac{d\phi_{\rm b}}{dt}$, we must multiply by $\frac{ds_{\rm b}}{dt}$. However, $\frac{ds_{\rm b}}{dt}$ and $\frac{ds_{\rm p}}{dt}$ are not constant throughout the orbit like $\frac{d\phi_{\rm b}}{dt}$ is in the face-on case. In fact, at the most extreme points in the orbit, the value of $\frac{ds_{\rm b}}{dt}$ is 0. To account for this, we calculated the average value of $\frac{ds_{\rm b}}{dt}$,

$$\overline{\frac{ds_{\rm b}}{dt}} = \frac{2a\omega_{\rm b}}{\pi}, \tag{3.5}$$

and similarly for $\overline{\frac{ds_{\rm p}}{dt}}$ For this calculation, the semi-major axis $a_{\rm b}$ of the stellar binary orbit was taken to be $s_{\rm b}$ and similarly $a_{\rm p}$ as $s_{\rm p}$ for the planet's orbit. The Equation for $\Omega_{\rm E}$ is shown in equation Equation 3.6.

$$\Omega_{\rm E} = \frac{\left(\overline{\frac{dr_{\rm pc}}{ds_{\rm b}}}\right)\left(\overline{\frac{ds_{\rm b}}{dt}}\right)}{\left(\overline{\frac{dr_{\rm pc}}{ds_{\rm p}}}\right)\left(\overline{\frac{ds_{\rm p}}{dt}}\right)} = \frac{\left(\overline{\frac{dr_{\rm pc}}{ds_{\rm b}}}\right)}{\left(\overline{\frac{dr_{\rm pc}}{ds_{\rm p}}}\right)}\frac{a_{\rm b}\omega_{\rm b}}{a_{\rm p}\omega_{\rm p}} \tag{3.6}$$

Again, using the relation between angular velocities from Equation 3.3 and $a_{\rm b,p} = s_{\rm b,p}$, we arrive at the final calulation:

$$\Omega_{\rm E} = \left(\frac{\frac{dr_{\rm pc}}{ds_{\rm b}}}{\frac{dr_{\rm pc}}{ds_{\rm p}}}\right)\left(\frac{s_{\rm p}}{s_{\rm b}}\right)^{\frac{1}{2}} \tag{3.7}$$

The results of the calculations are shown in Figure 3.2. For the edge-on case, the movement of the planetary caustic due to the orbital motion of the stellar binary was always a small fraction of the movement due to the orbital motion of the planet. For the edge-on scenario, the close topologies have the largest relative fraction of planetary caustic motion due to the stellar binary. This effect is highest in close topologies because the planetary caustics undergo a much larger translation as $s_{\rm b}$ changes, as seen in Figure 2.7.

From the results here, the highest effects come from face-on, resonant caustics. For some of these systems, the planetary caustic motion due to the stellar binary would be as much as 10 times the motion from the planet. For these cases, it may be more likely for caustic motion to be detected, and thus more likely to detect that it is a circumbinary planet. However, in most cases the movement of the stellar binary doesn't allow us any additional significant chance to detect caustic motion.

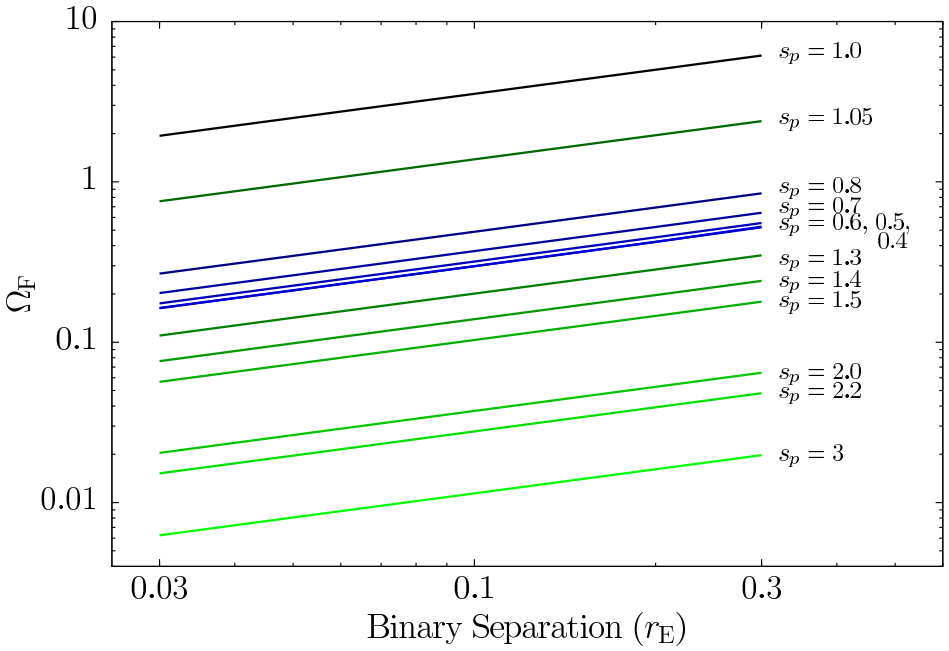

Fig. 3.1.— Comparitive caustic movement as the angle of the stellar binary, ϕ_b, changes corresponding to observing the system face-on. The bottom panel shows the caustic movement as the separation of the binary s_b changes, corresponding to observing the system edge-on. The colors provide a slightly easier view of the s_p values. Green indicates planetary separations greater than 1 r_E (wide topology), and blue indicates planet separations less than 1 r_E (close topology). The darker the shade of green or blue, the closer it is to 1 r_E.

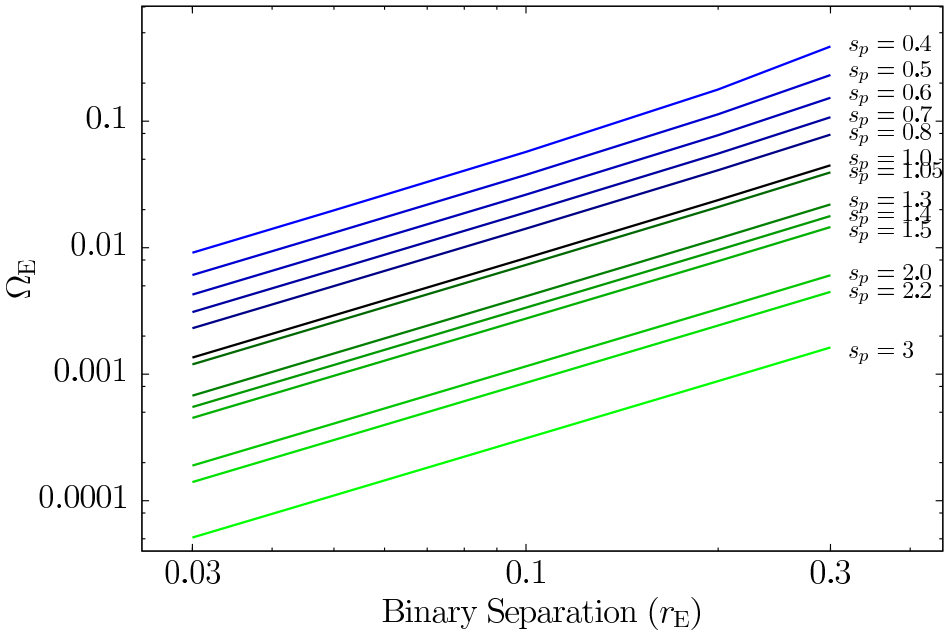

Fig. 3.2.— Comparitive caustic movement as the separation of the binary, $s_{\rm b}$, changes, corresponding to observing the system edge-on. The colors provide a slightly easier view of the $s_{\rm p}$ values. Green indicates planetary separations greater than 1 $r_{\rm E}$ (wide topology), and blue indicates planet separations less than 1 $r_{\rm E}$ (close topology). The darker the shade of green or blue, the closer it is to 1 $r_{\rm E}$.

Chapter 4: Fractional Detectability

The ultimate goal of this work is to obtain an estimation of the detectability of the circumbinary systems in microlensing. From examining the caustic structures we observe that for many source trajectories, the number of caustic crossings from the triple-lens is more than the number of caustic crossings for either of the double-lens approximations. One can easily notice this by imagining a trajectory that passes through the stellar binary portion of the caustics in Figure 2.3. We conclude that such trajectories would result in lightcurves that would be recognizable as triple-lens circumbinary systems. We posit that the fraction of source trajectories where this is true should be a lower limit on the fraction of lightcurves where the circumbinary nature will be recognizable.

This occurs with most frequency when the caustic is a resonant one because these are the largest caustics. This limits the range of $s_{\rm p}$ values to those very close to 1. To arrive at a fractional detectability for a given set of lens parameters, we arrange a grid of trajectories with various separations, u_0, and angles, α. We then calculate the number of caustic crossings along each trajectory for each of the three systems (triple-lens and two double-lens approximations). We describe how we count the number of caustic crossings using polygon clipping in Appendix A. If the number of crossings across the triple-lens caustic is less than or equal to the number of crossings along either of the double-lens approximations, we say that such a trajectory would not yield a lightcurve with recognizable triple-lens effects. Therefore, we say that the triple-lens system would only be detectable if it contains more caustic crossings than either double-lens system for a given trajectory. The fractional detectability is found by taking the fraction of trajectories with lightcurves that are detected from the total number of trajectories. Here it is important to acknowledge that this fractional detectability is probably a lower-limit. Presumably,

there would be many trajectories that do not explicitly cross a caustic, but would still pass close enough that the features would still be noticeable in the lightcurve. It is reasonable to expect that some of those trajectories that would not lead to detection by this particular method could still be recognized as triple-lens systems from the lightcurves.

4.1. Results

To determine the appropriate number of trajectories to use, we started with a small grid of trajectory separations (closest approach), u_0, and trajectory angles, α, and continually doubled the number of both until the fraction of detected trajectories started to converge. We found that this occured at 80 α's and 320 u_0's. This means there were 25,600 trajectories in our grid. We generated these trajectories across 6 values of $s_{\rm b}$, 3 values of $s_{\rm p}$, and 18 values of $\phi_{\rm b}$ (every 10°)[1]. We noticed that the angle of the stellar binary, $\phi_{\rm b}$, did not affect the fraction significantly, so we averaged the fraction detected over the 18 angles. This left us with 18 circumbinary systems (6 $s_{\rm b}$, 3 $s_{\rm p}$) for which we obtained a fraction of trajectories that would be detected. Figure 4.1 shows the caustic structures of these 18 circumbinary systems, the caustics of the corresponding double-lens approximations, and the fraction of trajectories that would lead to a detected circumbinary system. The figure can also be used as a visual for the limits of the superposition of the AB and Ab systems.

As can be seen from the plot, the fraction is highest when the stellar caustic and the planetary caustic are of similar size. In the regime where one caustic is larger than the other, the larger caustic dominates and there are fewer trajectories that would be detected as circumbinary. For most of the systems here, the fraction of trajectories that led to detected circumbinary systems was between 0.1 and 0.5. This suggests that circumbinary planets would be detectable for a large number of cases. Given that this should be a lower-limit of the fraction that are truly detectable, it is well within reason that microlensing is a technique capable of detecting circumbinary planets.

[1]For $q_{\rm b} = 1$, the systems have symmetry around 180°

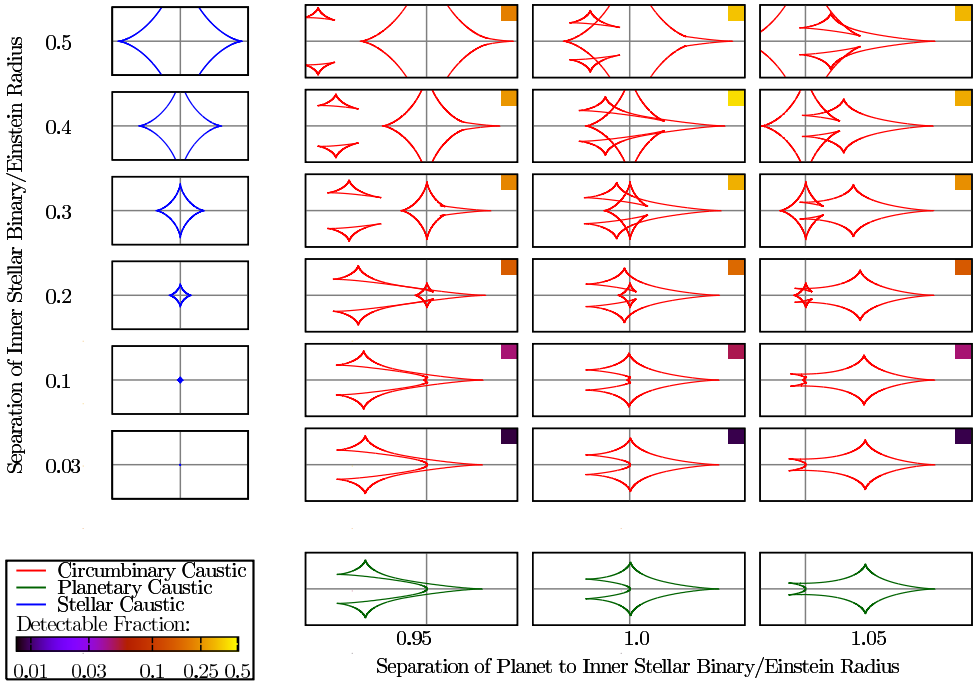

Fig. 4.1.— Caustic structures of circumbinary systems and fraction of trajectories detected. This plot shows the evolutions of the caustic structures are we change the separation of the planet and the separation of the inner binary. By comparing the stellar and planetary caustics with the circumbinary caustics with the same planet and stellar separation, we can see how the circumbinary caustics are a superposition of the two-body systems. The color of the boxes in the top right corner of the circumbinary plots indicate the fraction of trajectories that would produce noticeable circumbinary features (i.e. additional caustic crossings) and lead to detection.

Chapter 5: Summary and Discussion

This work has provided an in-depth look at microlensing in circumbinary systems. Although they are not new systems, circumbinary planets have yet to be discovered through the microlensing technique. Detecting a population of circumbinary planets with the microlensing method would show that circumbinary planets can be formed over a wide range of orbital separations. It could also have a great impact on various formation theories, perhaps even going beyond specifically circumbinary planet formation to our understanding of planet formation in general.

The majority of the focus of this work has been on the caustic structure of circumbinary systems. Understanding the caustics is a crucial first step in understanding potential circumbinary microlensing events. To do this, we explored a large section of the parameter-space for circumbinary systems, creating a collection of animations that show the effects of changing the parameters of the stellar binary. Circumbinary systems produce interesting features that are not seen in more simple double-lens microlensing, and by examining these features, we can begin to gain an intuitive sense of the range of parameters that produce interesting caustics.

From the animations, it is evident that the position of the stellar binary plays an important role in the structure of the caustics. Since the binary star orbits more quickly than the planet it is reasonable to expect that the motion of the stellar binary could produce a change in the caustic over the duration of the microlensing event. We therefore investigated the relative motion of the planetary caustics due to the orbit of the stellar binary and the orbit of the planet. We find that in most cases, the movement of the caustics due to the orbital motion of the stellar binary is a small fraction of the movement caused by the orbital motion of the planet. We conclude that there is little danger of confusing binary induced caustic motion for

planetary orbital motion, except in systems where the caustic structure itself will likely reveal the circumbinary nature of the lens.

Our final analysis quantified the detectability of circumbinary systems. We defined a detectable circumbinary event as one where the source trajectory contains more caustic crossings than in either of the two double-lens approximations. By examining a large number of trajectories across resonant caustics, we were able to obtain estimations for the detectability of given caustics. We show that for the systems where microlensing is most sensitive, circumbinary planets could be detected as such up to 50% of the time. These results show that microlensing is more than capable of detecting circumbinary planets.

With these results, it is important to put them in context. While it is true that the fraction we present is likely to be a lower limit, the range of parameters covered is very limited. We have explored only the resonant caustics, and therefore have looked only at circumbinary planets that have separations very close to that of the Einstein radius. The result then is that this is an optimistic number, and represents microlensing's most sensitive areas. For close and widely separated planets, the fraction would be significantly different. However, this work was meant to determine if circumbinary planets could be detected as such in microlensing, which is why we chose to look at the resonant caustics. These results prove that circumbinary planets can certainly be detected through microlensing techniques.

These results also bring up an interesting question. With such relatively high fractional detectabilities, why have no circumbinary planets been discovered through microlensing so far? This appears to have several answers. First, as described above, this is a somewhat optimistic result, as we have examined the region of parameter-space where microlensing would be most sensitive. Second, there is very little precedent for discovering triple-lens microlensing events. To date, only four triple-lens events have been discovered, two of which occurred last year (Gaudi et al. 2008; Han et al. 2013; Gould et al. 2014; Poleski et al. 2014). One could suggest that it was a lucky year for triple-lens events. However, it appears to be a result of both denser, more precise coverage and better ability to fit triple-lens models. That said, microlensing does depend largely on luck, and the chance alignment of a

system with a background star. With the relatively small number of microlensing events that occur, it is not surprising that only a small number are found to be in triple lens systems.

Finally, it is entirely possible a microlensing event from a circumbinary system has been observed. However, it may have been misidentified due to a number of different reasons. A simple scenario is one in which the stellar caustic component was very small and unable to be detected. The same could be true if the planetary componenet was very small. Another scenario is one where the stellar and planetary componenents of the caustic are of equal size, but the source trajectory happens to pass where one of the components is dominated by the other. Finally, if the observed data is poor and sparse, then even with optimal alignment and source trajectories, the data may be better fit by a double-lens. These scenarios are especially likely to occur if the binary star lensing features dominate the lightcurve, as these events typically do not get rigorously modeled.

In any event, the advent of better microlensing observations and data analysis is promising for the detection of circumbinary planets in microlensing. Microlensing is hitting its stride, and future events should be covered with much more precision. Additionally, future microlensing surveys like the Korean Microlensing Telescope Network (KMTNet) (Henderson et al. 2014), and the Wide Field Infrared Space Telescope (WFIRST) (Spergel et al. 2015) will allow for better data, and should increase the number of detected microlensing events.

5.1. Future Work

There are a number of plans to extend this project, most of them aimed at expanding the detectability fraction. The first goal is to explore the detectability for circumbinary systems where the binary stars do not have the same mass (i.e. $q_{\rm b} \neq 1$). From a preliminary look, it appears that this should not widely affect the detectability in a negative way, except in the case where one star is significantly more massive than the other. For those cases, the systems may be more likely to be misidentified as multiplanet systems. A non-unity stellar mass ratio may also have

a positive effect on the detectability fraction by stretching out the features of the caustic that come from the AB system, allowing more trajectories to cross it.

In addition to looking at $q_{\rm b} \neq 1$, we wish to implement this technique over a wider range of parameters. In addition to simply looking at a wider range of $s_{\rm b}$ and $s_{\rm p}$, the goal is to make several copies of Figure 4.1 for a range of $q_{\rm p}$ values as well. Now that this method has been implemented, it will be easier to not only search over a wider range of parameters, but also to sample the parameters more densely.

A somewhat similar approach to detectability could also be applied to lightcurves, rather than caustics. Because the lightcurves are the observed result of a microlensing event, it is necessary to extend the question of detectability to the lightcurves themselves. One method of doing so would be to generate lightcurves from a similar grid of trajectories for a wide range of ABb systems. If the generated lightcurves are fit well by AB or Ab lightcurves, then the ABb system would not be detected as such. Using this criterion, one could create a similar detectability fraction for ABb systems by examining the actual lightcurves.

References

Albrow M. D. et al., 2000, The Astrophysical Journal, 534, 894

Armstrong D. J., Osborn H., Brown D., Faedi F., Gómez Maqueo Chew Y., Martin D., Pollacco D., Udry S., 2014, eprint arXiv:1404.5617

Danek ., Heyrovsky ., 2015a, eprint arXiv:1501.06519

Danek ., Heyrovsky ., 2015b, eprint arXiv:1501.02722

Dominik ., 1998, Astronomy and Astrophysics

Gaudi B. S., 2012, Annual Review of Astronomy and Astrophysics, 50, 411

Gaudi B. S. et al., 2008, Science (New York, N.Y.), 319, 927

Gaudi B. S., Naber R. M., Sackett P. D., 1998, The Astrophysical Journal, 502, L33

Gould A., Loeb A., 1992, The Astrophysical Journal, 396, 104

Gould A. et al., 2014, Science (New York, N.Y.), 345, 46

Han C., 2008, The Astrophysical Journal, 684, 684

Han C., Chang H.-Y., An J. H., Chang K., 2001, Monthly Notices of the Royal Astronomical Society, 328, 986

Han C. et al., 2013, The Astrophysical Journal, 762, L28

Henderson C. B., Gaudi B. S., Han C., Skowron J., Penny M. T., Nataf D., Gould A. P., 2014, The Astrophysical Journal, 794, 52

Holman M. J., Wiegert P. A., 1999, The Astronomical Journal, 117, 621

Ioka K., Nishi R., Kan-ya Y., 1999, Progress of Theoretical Physics, 102, 983

Kley W., Haghighipour N., 2014, Astronomy & Astrophysics, 564, A72

Lee D., Lee C., Park B., Chung S., Kim Y., Kim H., Han C., 2008, The Astrophysical Journal, 672, 623

Mao S., Paczynski B., 1991, The Astrophysical Journal, 374, L37

Meschiari S., 2014, The Astrophysical Journal, 790, 41

Penny M. T., Mao S., Kerins E., 2011, Monthly Notices of the Royal Astronomical Society, 412, 607

Poleski R. et al., 2014, The Astrophysical Journal, 795, 42

Press ., Teukolsky ., Vetterling ., Flannery ., 1992, Cambridge: University Press

Ryu Y.-H., Chang H.-Y., Park M.-G., 2011, Monthly Notices of the Royal Astronomical Society, 412, 503

Song Y.-Y., Mao S., An J. H., 2013, Monthly Notices of the Royal Astronomical Society, 437, 4006

Spergel . et al., 2015, eprint arXiv:1503.03757

Witt ., 1990, Astronomy and Astrophysics (ISSN 0004-6361), 236, 311

Wolszczan A., Frail D. A., 1992, Nature, 355, 145

Zhu W., Gould A., Penny M., Mao S., Gendron R., 2014, The Astrophysical Journal, 794, 53

Appendix A: Calculating the Number of Caustic Crossings

Calculating the number of caustic crossings was instrumental to this work. However, it is not a simple calculation. Finding the position of the caustics is straightforward, and is done by solving the critical curve equation (Equation 1.4) and mapping back to the source plane using the lens equation (Equation 1.1). Determining if a trajectory has crossed the boundary to a caustic is somewhat trickier, and is usually calculated by the following method.

A.1. Method 1: Number of Images

As discussed in section 1.2, the caustic curves mark the boundaries between regions with different numbers of images. As a source crosses this boundary, the number of images increases or decreases by two. Therefore, one way to calculate a caustic crossing is to calculate the number of images at each point along the trajectory, and mark where the number of images changes. The number of images at a given source point can be found by solving the complex lens equation (Equation 1.1) for z, which is a 5th order polynomial for $N_l = 2$, and is 10th order for $N_l = 3$. These cannot be solved analytically and must instead be solved using a numerical routine such as the ZROOTS subroutine (Press et al. 1992). However, the solutions to the complex polynomial are not necessarily solutions to the lens equation and the roots of the polynomial must be substitued back into the lens equation to check if they are actual solutions. The number of roots that are real solutions to the lens equation gives the number of images at the source point. For a given trajectory, the lens equation must be solved along each point to determine where images are created or destroyed. By marking the places where the number of images changes, we can determine how many times a given trajectory crosses a caustic. While this method is reasonably time-effective for a small number of trajectories, this method was much too slow for the large number of trajectories needed for an accurate representation of all possible

trajectories that cross the caustic. It was simply too time-consuming to have to solve the lens equation for each point on all of the trajectories. Instead, we devised a different method to calculate the number of caustic crossings that allowed us to only use ZROOTS once for each of the three systems: ABb, AB, and Ab.

A.2. Method 2: General Polygon Clipping

Due to the lengthy time to calculate the caustic crossings given by Method 1 we needed a way to quickly input a trajectory and calculate the number and positions of the places where the trajectory crosses a caustic. We devised a method which used the General Polygon Clipper library (`http://www.cs.man.ac.uk/~toby/gpc/`) to calculate the caustic crossings. For this method, the caustics of the ABb, AB, and Ab systems are found once. This is done by finding the critical curve (Equation 1.4) using ZROOTS for the first value of ψ and then using Newton's Method to find the rest of the roots in order. By putting the roots back through the lens equation, we can obtain each corresponding point along the caustic.

Once the roots to the Jacobian equation are found, is important that the roots are left unsorted so that the same root number for each ψ value corresponds to the same part of the caustic. The roots then need to be linked together to form an array for the caustics. For this case, we were only concerned with the caustics that could merge to form a resonant caustic, and for that reason, we only considered the first four of six roots. The final two roots correspond to the distant caustics produced by the stellar binary (the bottom right panel of Figure 2.2). Once we have arrays for each the caustic positions of the four roots, it was necessary to link them together to form one continuous array for the resonant caustic. However, in some of the systems, the caustics were not fully merged at $s_{\rm p} = 1$, but instead the two planetary caustics were very close to the central caustic. In order to account for this, we first had to search through the four arrays of roots to find caustics that were self-linked, by simply checking if the first and last point in the array were the same point. After identifying the self-linked caustics, we then linked the remaining caustics together by matching up final points in one array to the initial points in other arrays. This is shown in Figure A.1.

What we are left with is an array for each closed caustic. The next step is to transform these into a GPC polygon. GPC polygons are capable of containing several 'contours' for a given polygon. This enabled us to simply store each caustic array as a different contour and have them all be a part of the same polygon. When the polygon is clipped using the intersection function, all contours are checked for intersection.

Once we have polygons that correspond to the caustics for the ABb, AB, and Ab systems, we can generate the proper trajectories. For a given trajectory, we create a polygon (for simplicity we used a rectangle) where one side is the line of the trajectory. Using the clipping function in the GPC library, we are able to find the resulting polygon from the intersection of the caustic polygon with the trajectory polygon. Figure A.2 shows the result of clipping two polygons. We can then quickly search through the points of of the resulting polygon to find the points that lie on the original trajectory. This method is about an order of magnitude faster than the Method in A.1, since it requires less computation, and the caustic only needs to be computed once for each system. As a result, this method could easily be applied to systems with even more masses without requiring very much additional computing time, given that the critical curve polynomial is of order $2N_l$, whereas the lens equation is of order $5N_l - 5$.

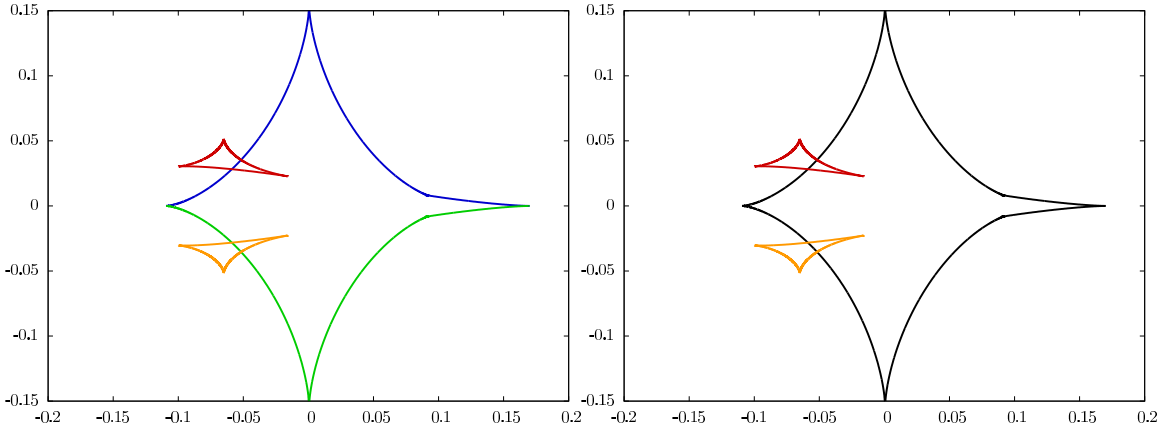

Fig. A.1.— Example of linking roots in the caustic. After solving the Jacobian equation, the caustics are arranged by root. In the left panel, the different colors correspond to different root numbers. The right panel shows the result after linking the roots by caustics. Each color now corresponds to a closed caustic. Each of the closed caustics becomes its own contour in the GPC polygon.

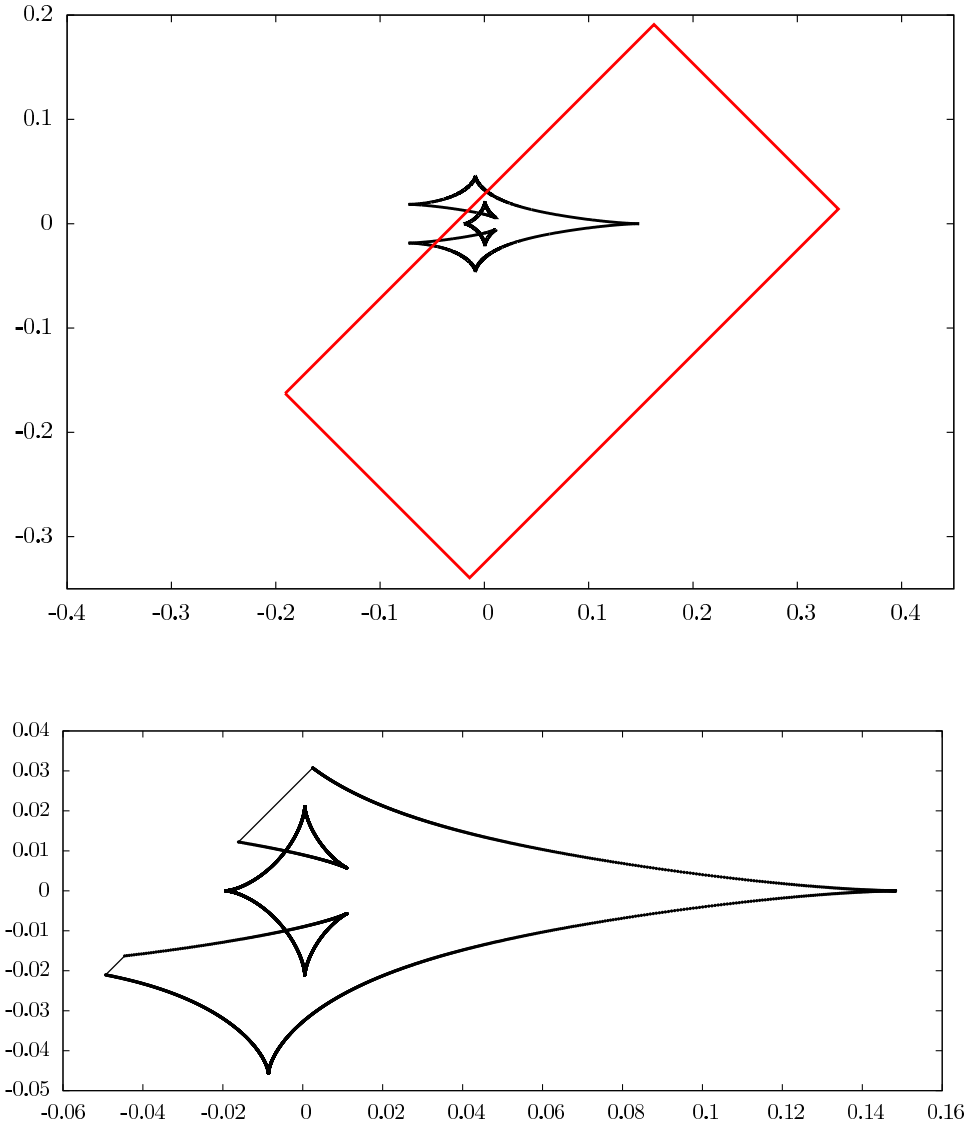

Fig. A.2.— Example of how the polygon clipper works to find the number of caustic crossings. The black curves show the ABb caustic with parameters $q_{\rm b} = 1$, $s_{\rm b} = 0.2\ r_{\rm E}$, $\phi_{\rm b} = 0$, $s_{\rm p} = 1\ r_{\rm E}$, and $q_{\rm p} = 10^{-3}$. The top panel shows the ABb caustic polygon with the trajectory polygon in red. The bottom panel shows the result of clipping the two polygons. The thinner black lines in the bottom panel indicate spaces between points in the polygon array. Therefore, the number of caustic crossing can be determined by searching through the clipped polygon and finding the points that lie along the original trajectory line.